**ORIGINAL ARTICLE**

**Open Access**

# Dual-assisted high-precision tracking technique for wideband multiplexed signals in new generation GNSS

Yunhan Qi[1], Zheng Yao[1,2*] and Mingquan Lu[1,2]

## Abstract

With the evolution of Global Navigation Satellite System (GNSS), new generation GNSS signals have adopted the dual-frequency multiplexing modulation techniques, which jointly modulate multiple signals located on multiple sub-frequencies into a Wideband Multiplexed Signal (WMS). Although WMSs were proposed initially to reduce the complexity of satellite transmitters and improve the transmission efficiency of signals, their multi-component structures and wide root mean square bandwidths introduced by high-frequency subcarriers also provide the possibility to improve the GNSS ranging precision. Therefore, this paper proposes a Dual-assisted Multi-component Tracking (DMT) technique, which can not only fully use high-frequency subcarriers in WMSs, but also effectively track carrier, subcarrier, and code by jointly utilizing all components in WMS. In this paper, the tracking and ranging performances of DMT are comprehensively analyzed theoretically and by simulation and real experiments. The results show that compared with existing WMS tracking methods, DMT can achieve tracking results with lower tracking jitters and ranging results with higher precision, providing a highly advantageous solution for new generation GNSS signal processing.

**Keywords**  Wideband multiplexed signal, Dual-assisted, Multi-component, High precision tracking

## Introduction

With the increasing demands of Global Navigation Satellite System (GNSS) to provide reliable and high precision positioning, navigation, and timing services and the limited GNSS spectrum resources, new generation GNSSs plan to broadcast multiple signals located on multiple sub-frequencies with complex spreading modulations and data-plus-pilot component structures in each transmission band (Dunn & Disl, 2019; Hein, 2020; Lu et al., 2019; Rebeyrol et al., 2007; Wu et al., 2020). To ensure the consistency of multiple signals in the same transmission band and relieve the complexity of satellite transmitters, the signals on multiple sub-frequencies in the same transmission band will be jointly modulated and broadcast. Currently, the signals, broadcast in Galileo Navigation Satellite System (Galileo) E5 band, the third generation BeiDou Navigation Satellite System (BDS-3) B1 band and BDS-3 B2 band, adopt the dual-frequency multiplexing modulation techniques (Lestarquit et al., 2008; Yao et al., 2017a; Yao et al., 2016). Such signals can be referred to the Wideband Multiplexed Signal (WMS). Figure 1 exhibits the spectrums of E5 WMS composed of Galileo E5a and E5b, B2 WMS composed of BDS-3 B2a and B2b, and B1 WMS composed of BDS-3 B1I and B1C. As the figure shows, these WMSs with dual-frequency

*Correspondence:
Zheng Yao
yaozheng@tsinghua.edu.cn
[1] Department of Electronic Engineering, Tsinghua University, Beijing 100084, China
[2] Beijing National Research Center for Information Science and Technology, Beijing 100084, China

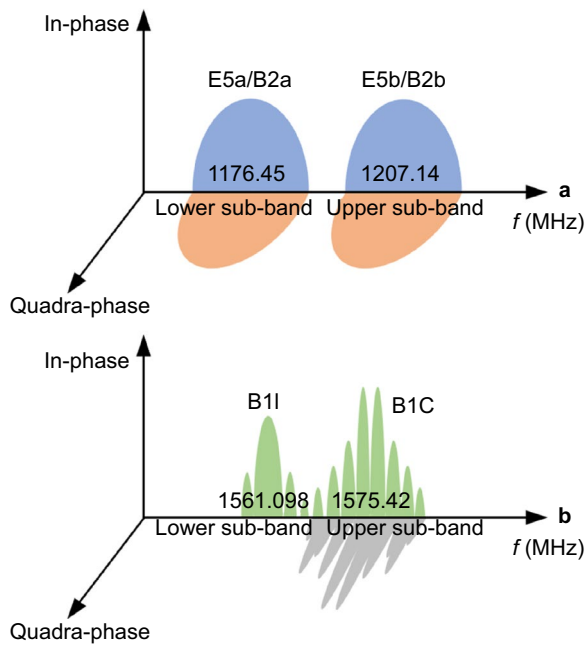Qi *et al. Satellite Navigation*        (2024) 5:5

Page 2 of 22



**Fig. 1** The spectrums of **a** E5 WMS and B2 WMS, and **b** B1 WMS

multiplexing modulations are composed of the components located on two adjacent sub-frequencies, which are referred to the lower sub-band components and upper sub-band components. On one hand, dual-frequency multiplexing modulation techniques adopted by WMSs ensure that the satellite transmitters can broadcast the signals with low implementation complexity and high transmission efficiency. On the other hand, multi-components on multi-sub-frequencies in WMSs also provide various options for receiving and processing these signals for GNSS receivers (Yao et al., 2017b).

For GNSS receivers, in consistence with traditional single-frequency GNSS signal processing, lower sub-band components and upper sub-band components in WMSs can be treated as two single-frequency GNSS signals and thus be separately received and processed (Gao et al., 2019; Shivaramaiah et al., 2009). Since the carrier, subcarrier, and code phases of lower and upper sub-band components are coherent according to dual-frequency multiplexing modulation techniques ((Lestarquit et al., 2008; Yao et al., 2017a; Yao et al. 2016), both lower and upper sub-band components have the potential to be jointly processed (Linty et al., 2020). More specifically, for broadcasting multiple components on two adjacent sub-frequencies, WMSs adopt the high-frequency subcarriers between lower and upper sub-bands. Therefore, the power main lobes of lower and upper sub-band components are located on two sub-frequencies with a large frequency difference, which implies the splitter spectrum

characteristics, thus wider Root Mean Square Bandwidths (RMSB) and higher precision ranging potential of WMSs (Gao et al., 2020b). Besides, because of more components with the coherences in carrier, subcarrier, and code phases in WMSs, the joint utilization of these components can further improve the tracking and ranging precisions. Therefore, to take full advantages of WMSs in high precision tracking and ranging, tracking techniques should utilize not only the high-frequency subcarriers between lower and upper sub-bands fully, but also all the components in WMSs effectively for joint tracking.

The existing WMS tracking techniques can be divided into two categories according to the local carriers used in tracking, which are the symmetric subcarrier method whose local carrier is the center sub-frequency of lower and upper sub-bands (Chen et al., 2013; Ren et al., 2012; Shivaramaiah & Dempster, 2009; Tawk et al., 2012; Wang et al., 2017; Yan et al., 2018; Zhou & Pan, 2014; Zhu et al., 2015), and the asymmetric subcarrier method whose local carrier is the sub-frequency of upper sub-band (Gao et al., 2020a, c). Although both symmetric and asymmetric subcarrier methods track the same WMSs, the equivalent baseband WMSs tracked by these two kinds of methods are different due to their different local carriers used in tracking, thus having different tracking structure characteristics.

For the symmetric subcarrier methods, since the used local carriers are the center sub-frequencies between lower and upper sub-bands, the lower and upper sub-band components in equivalent baseband WMS are modulated by the subcarrier whose frequency is half the frequency differences between upper and lower sub-bands. Taking the B2 WMS as an example, the local carrier frequency used in the symmetric subcarrier methods is 1191.795 MHz, and thus the subcarrier frequency for lower and upper sub-band components is ±15.345 MHz. More specifically, the symmetric subcarrier methods (Shivaramaiah & Dempster, 2009; Tawk et al., 2012; Zhou & Pan 2014) proposed for E5 WMS treat the lower sub-band components E5a and upper sub-band components E5b, which are modulated by the subcarrier with the frequency of 15.345 MHz, as a whole for joint processing. The side-peak cancellation methods based on cross-correlation functions (Chen et al., 2013; Yan et al., 2018) are also proposed to relieve the ambiguity problems introduced by the subcarriers in E5 WMS tracking. Unlike (Chen et al., 2013; Shivaramaiah & Dempster, 2009; Tawk et al., 2012; Yan et al., 2018; Zhou & Pan, 2014), the symmetric subcarrier methods proposed in (Ren et al., 2012; Wang et al., 2017; Zhu et al., 2015) adopt the two-dimensional tracking techniques, such as Dual Estimator Tracking (DET) (Hodgart & Simons, 2012) and Dual Phase Estimator (DPE) (Borio, 2014), to track the subcarrier

and code of WMSs separately (Ren et al., 2012) combines the code of lower and upper sub-band components and utilizes the DET to extract subcarrier phases. A Dual Binary-phase-shifting-keying Tracking (DBT) method proposed in (Zhu et al., 2015) utilizes a lower sub-band component and an upper sub-band component for joint discriminations and adopts the DPE to derive subcarrier phases. Like (Zhu et al., 2015), (Wang et al., 2017) converts the components with unequal power in B1 WMS to the components with equal powers by power normalizations, so that the DBT proposed by (Zhu et al., 2015) can be implemented to extract subcarrier phases.

For the asymmetric subcarrier methods, since the used local carrier is the upper sub-band sub-frequency, the lower sub-band components in equivalent baseband WMSs are modulated by the subcarrier whose frequency is the frequency difference between lower and upper sub-bands, while the upper sub-band components in equivalent baseband WMS signals are not modulated by such subcarriers. Taking the B2 WMS as an example, the local carrier frequency is 1207.14 MHz, subcarrier frequency of lower sub-band components is −30.69 MHz and the subcarrier frequency of upper sub-band components is 0 MHz. To accurately extract the subcarrier phases in equivalent baseband WMSs with asymmetric subcarriers, (Gao et al., 2020c) and (Gao et al., 2020a) propose a Cross Assisted Tracking (CAT) method based on DPE, which utilizes an upper sub-band component to track carrier and a lower sub-band component to track subcarrier and code.

The two kinds of WMS tracking methods differ in two aspects. In the aspect of utilizing spectrum separation characteristics of WMSs, the existing WMS tracking methods process the same WMS, but different local carriers adopted by WMS tracking structures imply different equivalent baseband WMSs, thus indicating different RMSBs and different ranging performances of equivalent baseband WMSs. However, the existing RMSBs of equivalent baseband WMS are all designed for the symmetric tracking method whose local carrier frequency is center sub-frequency between lower and upper sub-bands (Betz & Kolodziejski, 2009a, b). When the local carrier takes other values, the RMSBs of corresponding equivalent baseband WMS cannot be directly derived. Therefore, the theoretical tracking performance of two kinds of methods cannot be fully analyzed and compared, implying that the optimal utilization of the spectrum separation characteristics of WMSs remains to be further explored.

In the aspect of utilizing multiple components in WMSs for tracking, for the asymmetric subcarrier methods, since only the lower sub-band components, but not the upper ones, in equivalent baseband WMS are modulated by subcarrier, they intrinsically cannot utilize both upper and lower sub-band components for subcarrier tracking. For symmetric subcarrier methods, both the lower and upper sub-band components of equivalent baseband WMS are modulated by two subcarriers with the symmetric frequency, thus they can track jointly. However, most of the existing multi-component tracking methods (Julien, 2005; Tran, 2004; Tran & Hegarty, 2002; Yao et al., 2009) utilize only two components. The joint tracking with more than two components has not been clearly articulated.

Therefore, to take advantages of the high precision tracking and ranging potential of WMSs, this paper proposes a Dual-assisted Multi-component Tracking (DMT) technique. The main contributions of this paper are summarized as follows:

- This paper proposes a theoretical analysis method for WMS tracking with an arbitrary local carrier. More specifically, it designs an extended RMSB for equivalent baseband WMS to quantitatively analyze the ability of WMS tracking structures by taking advantage of spectrum separation characteristics. Based on this, from the perspective of tracking Cramer-Rao Lower Bound (CRLB), this paper also optimizes the WMS tracking structure in the aspect of both spectrum separation and multi-component characteristics, providing significant guidance to the design of WMS tracking structure.
- This paper proposes a DMT technique. On one hand, the specifically designed dual-assisted tracking structure in DMT can use not only WMS's spectrum separation characteristics, but also both the lower and upper sub-band components for joint tracking. On the other hand, DMT specifically designs a multi-component joint tracking based on an optimal thermal noise criterion. Theoretical analysis and experiment results show that compared with the existing WMS tracking methods, DMT can achieve lower tracking jitters and derive higher precision observations.

In this paper, we first introduce the WMS model and its properties. Next, we introduce the theoretical analysis method for WMS tracking with arbitrary local carriers and optimize the WMS tracking structure based on CRLB. Then, we introduce the design principles of DMT and the implementations of carrier, subcarrier, and code tracking loops in DMT, and comprehensively assess the tracking and ranging performances of DMT by theoretical, simulation, and real data analysis. Finally, conclusions will be discussed.

## Wideband multiplexed signal

This section will introduce the model and properties of WMS. Ignoring the inter-modulations used to maintain signal's constant envelopes (Lestarquit et al., 2008; Yao et al., 2017a, Yao et al., 2016), the WMS broadcast by the satellite can be modeled as

$$
\begin{aligned}
s_{\mathrm{RF}}(t) &= \mathrm{Re}\left\{ \sum_{x\in\{l,u\}} \sum_{i=1}^{N_x} s_x^{(i)}(t) \right\} \\
&= \mathrm{Re}\left\{ \sum_{x\in\{l,u\}} \sum_{i=1}^{N_x} \sqrt{P_{s,x}^{(i)}} d_x^{(i)}(t) g_x^{(i)}(t) e^{\left(2\pi f_x t + \phi_x^{(i)}\right)} \right\} \\
&= \sum_{x\in\{l,u\}} \sum_{i=1}^{N_x} \sqrt{P_{s,x}^{(i)}} d_x^{(i)}(t) g_x^{(i)}(t) \cos\left(2\pi f_x t + \phi_x^{(i)}\right)
\end{aligned}
\tag{1}
$$

where $x \in \{l,u\}$ represents the lower and upper sub-band, respectively, $s_x^{(i)}(t)$ is the $i$th component in $x$ sub-band, $f_x$ and $N_x$ are the sub-frequency and the component numbers of $x$ sub-band, respectively, $P_{s,x}^{(i)}$, $d_x^{(i)}(t)$, $g_x^{(i)}(t)$ and $\phi_x^{(i)}$ are the component power, navigation bit or secondary code, baseband spreading code, and initial phase of $s_x^{(i)}(t)$, respectively. According to dual-frequency multiplexing modulation techniques (Lestarquit et al., 2008; Yao et al., 2017a, Yao et al., 2016), since components in WMS are synchronous, all these components have coherent phase relationships. Table 1 lists the model parameters of E5 WMS, B1 WMS and B2 WMS.

When receiving WMSs, on one hand, since all the components in WMSs share the same transmission channel in free space, the each component of the received WMSs has the same signal propagation delay, and the coherent relationships on component phases and powers are also maintained. On the other hand, although the Dopplers of lower sub-band components and upper sub-band components are different due to the different sub-band sub-frequencies, lower sub-band Doppler and upper sub-band Doppler are related because both of them reflect the relative motion between the same satellite and the same receiver. Therefore, the received WMS can be expressed as

$$
\begin{aligned}
r(t) &= \sum_{x\in\{l,u\}} \sum_{i=1}^{N_x} \left\{ r_x^{(i)}(t) \right\} + n(t) \\
&= \sum_{x\in\{l,u\}} \sum_{i=1}^{N_x} \left\{ \sqrt{P_x^{(i)}} d_x^{(i)}(t-\tau) g_x^{(i)}(t-\tau) \cos\left(2\pi\left(f_x + f_x^d\right)(t-\tau) + \phi_x^{(i)}\right) \right\} \\
&\quad + n(t)
\end{aligned}
\tag{2}
$$

where $r_x^{(i)}(t)$ is the received $i$th component in $x$ sub-band, $P_x^{(i)}$ and $f_x^d$ are the received component power and Doppler of $r_x^{(i)}(t)$ respectively, $\tau$ is the signal propagation delay, and $n(t)$ is the zero-mean Gaussian noise with Power Spectral Density (PSD) of $N_0$.

According to (1), (2) and the spectrums exhibited in Fig. 1, WMSs have three main characteristics:

- **Spectrum separation characteristics**: the power spectrum main lobes of lower and upper sub-band components are located at two sub-frequencies which have a large frequency difference. Therefore, compared with the traditional single-frequency GNSS signals, WMSs have much splitter spectrums, indicating the wider RMSBs and higher precision ranging potentials.
- **Multi-component characteristics**: compared with the traditional single-frequency GNSS signals, there are more components in WMSs. For example, the B2 WMS has four components while both B2a and B2b only have 2 components. Therefore, the track-

**Table 1** Model parameters of E5 WMS, B1 WMS and B2 WMS

| Signal type | Sub-band | $N_x$ | $f_x$ (MHz) | $g_x^{(i)}$ | Modulation | $\phi_x^{(i)}$ (°) |
|---|---|---|---|---|---|---|
| E5 WMS | Lower | 2 | 1176.45 | $g_l^{(1)}$ | BPSK(10) | 0 |
| | | | | $g_l^{(2)}$ | BPSK(10) | 90 |
| | Upper | 2 | 1207.14 | $g_u^{(1)}$ | BPSK(10) | 0 |
| | | | | $g_u^{(2)}$ | BPSK(10) | 90 |
| B1 WMS | Lower | 1 | 1561.098 | $g_l^{(1)}$ | BPSK(2) | 0 |
| | Upper | 2 | 1575.42 | $g_u^{(1)}$ | BOC(1,1) | 0 |
| | | | | $g_u^{(2)}$ | QMBOC(6,1,4/33) | 90 |
| B2 WMS | Lower | 2 | 1176.45 | $g_l^{(1)}$ | BPSK(10) | 0 |
| | | | | $g_l^{(2)}$ | BPSK(10) | 90 |
| | Upper | 2 | 1207.14 | $g_u^{(1)}$ | BPSK(10) | 0 |
| | | | | $g_u^{(2)}$ | BPSK(10) | 90 |

*BPSK* Binary phase shifting keying, *BOC* Binary offset carrier, *QMBOC* Quadratic multiplexed binary offset carrier

ing of WMSs can utilize more components, further improving the tracking and ranging precisions.

- **Signal coherence characteristics**: at the receivers and the satellites, the phase relationships, propagation delays and Dopplers of both lower and upper sub-band components in WMSs are coherent, providing the basis for joint reception and processing.

## Theoretical analysis method for WMS tracking

To theoretically analyze the performances of WMS tracking with different local carriers, this section first designs an extended RMSB for equivalent baseband WMS with an arbitrary local carrier. Based on this, this section will optimize the WMS tracking structure from the perspective of tracking CRLB which considers both RMSB and multi-components of WMS.

### Extended RMSB for equivalent baseband WMS with an arbitrary local carrier

To quantitively analyze the ability of WMS tracking structure to utilize WMS's spilt spectrum, RMSB of equivalent baseband WMS should be calculated. However, as mentioned before, since the existing theoretical analysis methods (Betz & Kolodziejski, 2009a; b) assume the local carrier frequency is the center sub-frequency between lower and upper sub-bands, that is $f_o = (f_l + f_u)/2$, these methods cannot be directly implemented when the local carrier takes other values.

Without the loss of generality, suppose the frequency of the local carrier is $f_o$ and the numbers of lower components and upper components involved in tracking are $\hat{N}_l \in [1, N_l]$ and $\hat{N}_u \in [1, N_u]$, respectively, the tracked WMS can be equivalently transformed by (2) and expressed as

$$r(t) = \sum_{x \in \{l,u\}} \sum_{i=1}^{\hat{N}_x} \left\{ \sqrt{P_x^{(i)}} d_x^{(i)}(t - \tau) g_x^{(i)}(t - \tau) \cos\left(2\pi f_o t + \varphi_o - 2\pi f_s^x t - \varphi_s^x + \phi_x^{(i)}\right) \right\} + n(t) \tag{3}$$

where $\varphi_o = -2\pi f_o \tau$ is the carrier phase, $f_s^x = f_o - f_x - f_x^d$ is the subcarrier frequency for $x$ sub-band components, and $\varphi_s^x = -2\pi f_s^x \tau$ is the $x$ sub-band subcarrier phase. Therefore, the equivalent baseband WMS can be expressed as

$$b(t) = \sum_{x \in \{l,u\}} \sum_{i=1}^{\hat{N}_x} b_x^{(i)}(t) + n(t)$$

$$= \sum_{x \in \{l,u\}} \sum_{i=1}^{\hat{N}_x} \left\{ \sqrt{P_x^{(i)}} d_x^{(i)}(t - \tau) g_x^{(i)}(t - \tau) \right.$$

$$\left. \cos\left(-2\pi f_s^x t - \varphi_s^x + \phi_x^{(i)}\right) \right\} + n(t) \tag{4}$$

Define the normalized PSD of $g_x^{(i)}(t)$ is $G_x^{(i)}(f)$. The normalized PSD of equivalent baseband component $b_x^{(i)}(t)$ can be approximated as $G_x^{(i)}(f + f_s^x)$. Therefore, the power of components involved in tracking and normalized PSD of the tracked equivalent baseband WMS can be approximated as

$$C_s \approx \sum_{x \in \{l,u\}} \sum_{i=1}^{\hat{N}_x} P_x^{(i)} \tag{5}$$

and

$$G_s(f) \approx \sum_{x \in \{l,u\}} \sum_{i=1}^{\hat{N}_x} \frac{P_x^{(i)}}{C_s} G_x^{(i)}(f + f_s^x) \tag{6}$$

respectively. Assuming that the receiver's radio-frequency front-end receives the WMS with the down-conversion frequency $f_r = (f_l + f_u)/2$ and the lower-pass filter one-side bandwidth $\beta_r$, the spectrum of the equivalent baseband WMS $b(t)$ with local carrier $f_o$ is exhibited in Fig. 2. Based on this, an extended RMSB of such an equivalent baseband WMS can be accordingly calculated as

$$\hat{\beta}_s = \sqrt{\int_{f_r - f_o - \beta_r}^{f_r - f_o + \beta_r} f^2 \eta^{-1} G_s(f) \, df}$$

$$= \sqrt{\int_{f_r - f_o - \beta_r}^{f_r - f_o + \beta_r} f^2 \eta^{-1} \sum_{x \in \{l,u\}} \sum_{i=1}^{\hat{N}_x} \frac{P_x^{(i)}}{C_s} G_x^{(i)}(f + f_s^x) \, df} \tag{7}$$
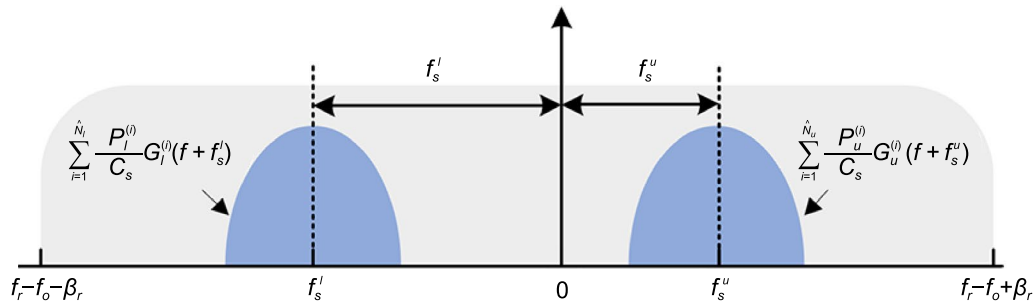
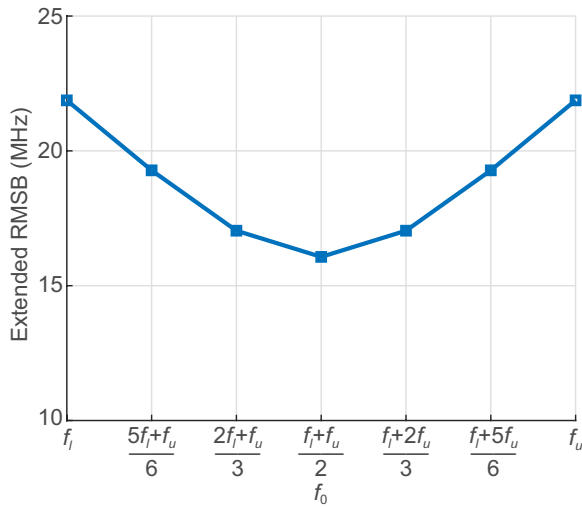**Fig. 2** Spectrum of equivalent baseband WMS $b(t)$ with the local carrier $f_o$



**Fig. 3** Extended RMSBs of equivalent baseband WMS with the example of E5 WMS when local carrier $f_o$ takes the value from $f_l$ to $f_u$ and $\beta_r = 36$ MHz

where

$$
\begin{aligned}
\eta &= \int_{f_r-f_o-\beta_r}^{f_r-f_o+\beta_r} G_s(f)\,\mathrm{d}f \\
&= \int_{f_r-f_o-\beta_r}^{f_r-f_o+\beta_r} \sum_{x\in\{l,u\}} \sum_{i=1}^{\hat{N}_x} \frac{P_x^{(i)}}{C_s} G_x^{(i)}\left(f+f_s^x\right)\,\mathrm{d}f
\end{aligned} \tag{8}
$$

is the remaining signal power ratio in limited bandwidth.

## Optimization of WMS tracking structure

Since the tracking CRLB considers both split spectrum and multi-component characteristics, it can be implemented to analyze the theoretical performance of WMS tracking with an arbitrary local carrier. According to classic tracking theory (Betz & Kolodziejski, 2009a; b) and extended RMSB in (7), the CRLB of WMS tracking with an arbitrary local carrier $f_o$ can be further expressed as

$$
\begin{aligned}
\sigma^2 &\cong \frac{B_{\mathrm{L}}(1-0.5B_{\mathrm{L}}T)}{(2\pi)^2 \eta \frac{C_s}{N_0} \hat{\beta}_s^2} \\
&\cong \frac{B_{\mathrm{L}}(1-0.5B_{\mathrm{L}}T)}{(2\pi)^2 \frac{C_s}{N_0} \int_{f_r-f_o-\beta_r}^{f_r-f_o+\beta_r} f^2 \sum_{x\in\{l,u\}} \sum_{i=1}^{\hat{N}_x} \frac{P_x^{(i)}}{C_s} G_x^{(i)}\left(f+f_s^x\right)\,\mathrm{d}f}
\end{aligned} \tag{9}
$$

where $B_{\mathrm{L}}$ is the loop filter bandwidth and $T$ is the pre-correlation time.

In the aspect of extended RMSBs of equivalent baseband WMS, ignoring the effect of Doppler and taking E5 WMS as an example, Fig. 3 exhibits the extended RMSBs of equivalent baseband WMSs when local carrier $f_o$ takes the value from $f_l$ to $f_u$ and $\beta_r = 36$ MHz. As the figure shows, when $f_o = (f_l + f_u)/2$, the equivalent baseband WMS has the minimal extended RMSB, which corresponds to the symmetric subcarrier method. When $f_o = f_u$, the extended RMSB of equivalent baseband WMS takes the maximum value, which corresponds to the asymmetric subcarrier method. Since the asymmetric subcarrier method has a wider extended RMSB than symmetric subcarrier method, the asymmetric subcarrier method can more fully exploit the spectrum separation characteristics compared with symmetric subcarrier method, thus providing higher precision tracking results. It should also be noticed that, when $f_o = f_l$, the extended RMSB of such a case is similar to that of the case with $f_o = f_u$. It means that the tracking results of WMS tracking methods with local carrier $f_o = f_l$ can be expected to have the similar high precision as the case with $f_o = f_u$. However, the case of $f_o = f_l$ has not been explored by the existing WMS tracking methods.

In the aspect of the component powers involved in tracking, all $N_l + N_u$ components in WMS should be utilized to avoid the tracking precision losses. When local carrier $f_o = f_u$, the lower sub-band components

are modulated by the subcarrier with the frequency of $f_u - f_l$, while the upper sub-band components have no such subcarrier modulation. Therefore, the tracking methods for this case, referred to the asymmetric subcarrier methods, can only utilize single sub-band components to track subcarrier, which intrinsically cannot utilize all the components in both lower and upper sub-band for joint tracking. When local carrier $f_o = (f_l + f_u)/2$, since the components in both lower and upper sub-bands are modulated by the subcarrier with the frequency of $(f_u - f_l)/2$, tracking methods for this case, referred to the symmetric subcarrier methods, can utilize all the components for joint tracking. However, most of the existing methods utilize one component in lower sub-band and one component in upper sub-band. The joint tracking with all the components from both lower and upper sub-bands has not been fully exploited.

According to above analysis, the optimal way to utilize WMS should *i)* have the largest extended RMSB of equivalent baseband WMS, *ii)* utilize both lower and upper sub-band components for joint tracking. However, although WMS tracking methods with local carrier $f_o = f_l$ or $f_o = f_u$ can make the best use of WMS's spectrum separation characteristics, they can only utilize single sub-band components in tracking, not dual sub-band components, resulting a loss of signal power. Moreover, even though WMS tracking methods can utilize all components of the upper and lower sub-bands for joint tracking, the specific joint tracking of multiple components has not been fully investigated. Therefore, in the next section, we will propose a tracking technique which can solve the above problems, achieving higher precision tracking and ranging.

## Dual-assisted multi-component tracking
This section first introduces the design principle of DMT. Then, the carrier, subcarrier and code tracking loops will be introduced in detail. Finally, the implementation of DMT will be discussed.

### Design principles
According to previous analysis, WMS tracking methods with local carrier $f_o = f_l$ or $f_o = f_u$ can make full use of spectrum separation characteristics of WMSs. Therefore, this subsection will design the proposed DMT by further analyzing the characteristics of correlations calculated by lower and upper sub-band components when $f_o = f_l$ and $f_o = f_u$.

*Correlation characteristics*
When the local carrier frequency is $f_u + f_u^d$ and all $N_l + N_u$ lower and upper sub-band components in WMS are utilized, the tracked WMSs can be obtained by reforming (3) as

$$
\begin{aligned}
r(t) = \sum_{i=1}^{N_l} &\left\{ \sqrt{P_l^{(i)}} d_l^{(i)}(t-\tau) g_l^{(i)}(t-\tau) \right. \\
&\left. \cos\left(2\pi f_o^u t + \varphi_o^u - 2\pi f_s t - \varphi_s + \phi_l^{(i)}\right) \right\} \\
+ \sum_{i=1}^{N_u} &\left\{ \sqrt{P_u^{(i)}} d_u^{(i)}(t-\tau) g_u^{(i)}(t-\tau) \right. \\
&\left. \cos\left(2\pi f_o^u t + \varphi_o^u + \phi_u^{(i)}\right) \right\} + n(t)
\end{aligned}
$$

(10)

where $f_o^u = f_u + f_u^d$ and $\varphi_o^u = -2\pi f_o^u \tau$ are the carrier frequency and phase respectively, and $f_s = f_u + f_u^d - f_l - f_l^d$ and $\varphi_s = -2\pi f_s \tau$ are the subcarrier frequency and phase, respectively.

According to (10), because of no subcarriers in upper sub-band components, tracking methods should utilize the upper sub-band components to estimate the carrier frequency $f_o^u$ and carrier phase $\varphi_o^u$. The correlations used in carrier tracking can be obtained by multiplying and integrating upper sub-band components with local carrier replica $\exp\left\{-j\left(2\pi \hat{f}_o^u t + \hat{\varphi}_o^u + \phi_u^{(i)}\right)\right\}$ and prompt local code replica $g_u^{(i)}(t - \hat{\tau})$ for upper sub-band components, which can be expressed as

$$
V_u^{(i)} = \frac{1}{T} \int_0^T r(t) g_u^{(i)}(t - \hat{\tau}) \exp\left\{-j\left(2\pi \hat{f}_o^u t + \hat{\varphi}_o^u + \phi_u^{(i)}\right)\right\} \mathrm{d}t
$$

(11)

where $\hat{\tau}$, $\hat{f}_o^u$, and $\hat{\varphi}_o^u$ are estimated $\tau$, $f_o^u$, and $\varphi_o^u$ respectively. Since lower sub-band components are modulated by subcarriers with frequency $f_s$, the tracking methods should utilize the lower sub-band components to track subcarrier and code. The corresponding correlations can be obtained by multiplying and integrating lower sub-band components with local carrier replica $\exp\left\{-j\left(2\pi \hat{f}_o^u t + \hat{\varphi}_o^u + \phi_l^{(i)}\right)\right\}$, local subcarrier replica $\exp\left\{+j\left(2\pi \hat{f}_s t + \hat{\varphi}_s\right)\right\}$, early, prompt, and late local code replica $g_l^{(i)}(t - \hat{\tau} + \delta_z)$ for lower sub-band components, which can also be expressed as

$$
\begin{aligned}
V_{l,z}^{(i)} = \frac{1}{T} \int_0^T &r(t) g_l^{(i)}(t - \hat{\tau} + \delta_z) \\
&\exp\left\{+j\left(2\pi \hat{f}_s t + \hat{\varphi}_s\right)\right\} \\
&\exp\left\{-j\left(2\pi \hat{f}_o^u t + \hat{\varphi}_o^u + \phi_l^{(i)}\right)\right\} \mathrm{d}t
\end{aligned}
$$

(12)

where $\hat{f}_s$ and $\hat{\varphi}_s$ are estimated subcarrier frequency and phase, $z \in \{E, P, L\}$ represents the early, prompt, and late brunch, $\delta_E = +\mu$, $\delta_P = 0$ and $\delta_L = -\mu$ are additional code phase delays. By calculating (11) and (12), upper and lower sub-band correlations are

$$V_u^{(i)} = \frac{\sqrt{P_u^{(i)}}}{2} d_u^{(i)} R_u^{(i)}(\Delta\tau) \mathrm{sinc}\big(\pi\Delta f_o^u T\big) \exp\big\{j\big(\pi\Delta f_o^u T + \Delta\varphi_o^u\big)\big\} \tag{13}$$

and

$$
\begin{aligned}
V_{l,E}^{(i)} &= \frac{\sqrt{P_l^{(i)}}}{2} d_l^{(i)} R_l^{(i)}(\Delta\tau - \mu) \mathrm{sinc}\big(\pi\big(\Delta f_o^u - \Delta f_s\big)T\big) \\
&\quad \exp\big\{j\big(\pi\big(\Delta f_o^u - \Delta f_s\big)T + \Delta\varphi_o^u - \Delta\varphi_s\big)\big\} \\
V_{l,P}^{(i)} &= \frac{\sqrt{P_l^{(i)}}}{2} d_l^{(i)} R_l^{(i)}(\Delta\tau) \mathrm{sinc}\big(\pi\big(\Delta f_o^u - \Delta f_s\big)T\big) \\
&\quad \exp\big\{j\big(\pi\big(\Delta f_o^u - \Delta f_s\big)T + \Delta\varphi_o^u - \Delta\varphi_s\big)\big\} \\
V_{l,L}^{(i)} &= \frac{\sqrt{P_l^{(i)}}}{2} d_l^{(i)} R_l^{(i)}(\Delta\tau + \mu) \mathrm{sinc}\big(\pi\big(\Delta f_o^u - \Delta f_s\big)T\big) \\
&\quad \exp\big\{j\big(\pi\big(\Delta f_o^u - \Delta f_s\big)T + \Delta\varphi_o^u - \Delta\varphi_s\big)\big\}
\end{aligned}
\tag{14}
$$

respectively, where $R_x^{(i)}(\cdot)$ is the Auto-Correlation Function (ACF) of $g_x^{(i)}(t)$, $\Delta\tau = \tau - \hat{\tau}$ is the propagation delay errors, $\Delta f_o^u = f_o^u - \hat{f}_o^u$ and $\Delta f_s = f_s - \hat{f}_s$ are frequency errors of carrier $f_o^u$ and subcarrier $f_s$, respectively, $\Delta\varphi_o^u = \varphi_o^u - \hat{\varphi}_o^u$ and $\Delta\varphi_s = \varphi_s - \hat{\varphi}_s$ are phase errors of carrier and subcarrier, respectively.

According to lower and upper sub-band correlations in (13) and (14), lower sub-band correlations $V_{l,E}^{(i)}, V_{l,P}^{(i)}, V_{l,L}^{(i)}$ in (14) have subcarrier frequency error $\Delta f_s$ and subcarrier phase error $\Delta\varphi_s$, while upper sub-band correlations $V_u^i$ in (13) have no any corresponding errors related with subcarriers, indicating that the lower sub-band correlations in (13) and upper sub-band correlations in (14) cannot be jointly used to track the subcarriers with frequency $f_s$.

### Dual-assisted tracking design of DMT

To utilize all the components in both lower and upper sub-bands for subcarrier tracking, the upper sub-band correlations are expected to have the same subcarrier frequency errors $\Delta f_s$ and subcarrier phase errors as the lower sub-band correlations, which means that the upper sub-band components should also be modulated by the subcarrier with the same frequency $f_s = f_u + f_u^d - f_l - f_l^d$.

According to previous theoretical analysis, when local carrier is $f_l + f_l^d$, the spectrum separation characteristics of WMS can also be fully utilized which is similar to the case of local carrier $f_u + f_u^d$. More specifically, when local carrier frequency equals $f_l + f_l^d$, in this equivalent baseband WMS, the lower sub-band components have no subcarriers while the upper sub-band components are modulated by the subcarriers with the frequency $f_u + f_u^d - f_l - f_l^d$, which is consistent with the lower sub-band subcarrier frequency when local carrier frequency is $f_o^u$. Therefore, when local carrier's frequency is $f_l + f_l^d$, the corresponding WMS has a dual form with (10), which can be expressed as

$$
\begin{aligned}
r(t) &= \sum_{i=1}^{N_l} \bigg\{ \sqrt{P_l^{(i)}} d_l^{(i)}(t - \tau) g_l^{(i)}(t - \tau) \\
&\quad \cos\big(2\pi f_o^l t + \varphi_o^l + \phi_l^{(i)}\big) \bigg\} \\
&\quad + \sum_{i=1}^{N_u} \bigg\{ \sqrt{P_u^{(i)}} d_u^{(i)}(t - \tau) g_u^{(i)}(t - \tau) \\
&\quad \cos\big(2\pi f_o^l t + \varphi_o^l + 2\pi f_s t + \varphi_s + \phi_u^{(i)}\big) \bigg\} + n(t)
\end{aligned}
\tag{15}
$$

where $f_o^l = f_l + f_l^d$ and $\varphi_o^l = -2\pi f_o^l \tau$ are carrier frequency and phase respectively. To distinguish two local carriers with frequencies $f_o^u$ and $f_o^l$, the carrier with frequency $f_o^l$ will be termed as the lower carrier, and the carrier with frequency $f_o^u$ will be termed as the upper carrier.

Like the calculation methods of lower and upper sub-band correlations in (11) and (12) when upper carrier $f_o^u$ is implemented, the upper and lower sub-band correlations, when lower carrier $f_o^l$ is used can be calculated by

$$
\begin{aligned}
V_{u,z}^{(i)} &= \frac{1}{T} \int_0^T r(t) g_u^{(i)}\big(t - \hat{\tau} + \delta_z\big) \\
&\quad \exp\big\{-j\big(2\pi\hat{f}_s t + \hat{\varphi}_s\big)\big\} \\
&\quad \exp\big\{-j\big(2\pi\hat{f}_o^l t + \hat{\varphi}_o^l + \phi_u^{(i)}\big)\big\} \mathrm{d}t
\end{aligned}
\tag{16}
$$

and

$$V_l^{(i)} = \frac{1}{T} \int_0^T r(t) \cdot g_l^{(i)}\big(t - \hat{\tau}\big) \exp\big\{-j\big(2\pi\hat{f}_o^l t + \hat{\varphi}_o^l + \phi_l^{(i)}\big)\big\} \mathrm{d}t \tag{17}$$

Qi *et al. Satellite Navigation*        (2024) 5:5

Page 9 of 22

respectively, where $\hat{f}_o^l$ and $\hat{\varphi}_o^l$ are estimated $f_o^l$ and $\varphi_o^l$, respectively. The correlations obtained by (16) and (17) can be written as

$$
\begin{aligned}
V_{u,\mathrm{E}}^{(i)} &= \frac{\sqrt{P_u^{(i)}}}{2} d_u^{(i)} R_u^{(i)}(\Delta\tau - \mu)\mathrm{sinc}\left(\pi\left(\Delta f_o^l + \Delta f_s\right)T\right) \\
&\quad \exp\left\{\mathrm{j}\left(\pi\left(\Delta f_o^l + \Delta f_s\right)T + \Delta\varphi_o^l + \Delta\varphi_s\right)\right\} \\
V_{u,\mathrm{P}}^{(i)} &= \frac{\sqrt{P_u^{(i)}}}{2} d_u^{(i)} R_u^{(i)}(\Delta\tau)\mathrm{sinc}\left(\pi\left(\Delta f_o^l + \Delta f_s\right)T\right) \\
&\quad \exp\left\{\mathrm{j}\left(\pi\left(\Delta f_o^l + \Delta f_s\right)T + \Delta\varphi_o^l + \Delta\varphi_s\right)\right\} \\
V_{u,\mathrm{L}}^{(i)} &= \frac{\sqrt{P_u^{(i)}}}{2} d_u^{(i)} R_u^{(i)}(\Delta\tau + \mu)\mathrm{sinc}\left(\pi\left(\Delta f_o^l + \Delta f_s\right)T\right) \\
&\quad \exp\left\{\mathrm{j}\left(\pi\left(\Delta f_o^l + \Delta f_s\right)T + \Delta\varphi_o^l + \Delta\varphi_s\right)\right\}
\end{aligned}
\tag{18}
$$

and

$$
V_l^{(i)} = \frac{\sqrt{P_l^{(i)}}}{2} d_l^{(i)} R_l^{(i)}(\Delta\tau)\mathrm{sinc}\left(\pi\Delta f_o^l T\right)\exp\left\{\mathrm{j}\left(\pi\Delta f_o^l T + \Delta\varphi_o^l\right)\right\}
\tag{19}
$$

respectively, where $\Delta f_o^l = f_o^l - \hat{f}_o^l$ and $\Delta\varphi_o^l = \varphi_o^l - \hat{\varphi}_o^l$ are the errors of lower carrier frequency and phase.

Since upper sub-band correlations $V_{u,\mathrm{E}}^{(i)}, V_{u,\mathrm{P}}^{(i)}, V_{u,\mathrm{L}}^{(i)}$ in (18) for lower carrier $f_o^l$ have the same subcarrier frequency error $\Delta f_s$ and phase error $\Delta\varphi_s$ as the lower sub-band correlations $V_{l,\mathrm{E}}^{(i)}, V_{l,\mathrm{P}}^{(i)}, V_{l,\mathrm{L}}^{(i)}$ in (14) for upper carrier $f_o^u$, the upper sub-band correlations in (18) and lower sub-band correlations in (14) can be jointly utilized to track the subcarriers with frequency $f_s$.

To calculate correlations in (14) and (18), WMS should multiply the upper carrier $f_o^u$ and lower sub-band components, the lower carrier $f_o^l$ and upper sub-band components. Therefore, a dual-assisted tracking structure can be summarized. The specifically designed dual-assisted tracking structure can best use not only WMS's spectrum separation characteristics, but also all the components in both lower and upper sub-bands for subcarrier tracking.

### *Multi-component joint tracking design of DMT*
To fully use each component's power, DMT will utilize the lower and upper sub-band correlations calculated by (13), (14), (18) and (19) to jointly track code, subcarrier, and carrier.

For the multi-component joint tracking in code and subcarrier, since the lower sub-band correlations $V_{l,\mathrm{E}}^{(i)}, V_{l,\mathrm{P}}^{(i)}, V_{l,\mathrm{L}}^{(i)}$ in (14) have the same code phase error and subcarrier phase error as the upper sub-band correlations $V_{u,\mathrm{E}}^{(i)}, V_{u,\mathrm{P}}^{(i)}, V_{u,\mathrm{L}}^{(i)}$ in (18), these correlations can be directly

used in code and subcarrier tracking. However, for the carrier tracking, since the Dopplers of lower and upper carriers are different, two carrier tracking loops are needed to separately track these two carriers. Although these two carriers are separately tracked, the Dopplers in both lower and upper carriers reflect the relative motion between the same receiver and the same satellite. Therefore, the lower carrier phase estimated by the multiple lower sub-band correlations $V_l^{(i)}$ in (19) and the upper carrier phase estimated by multiple upper sub-band correlations $V_u^{(i)}$ in (13) can be combined in the observation domain. The combined carrier phase is equivalent to the carrier phase estimated by utilizing all components in lower and upper sub-bands.

For multi-component joint tracking, we specifically design a multi-component joint tracking method based on an optimal thermal noise criterion. The designed multi-component tracking first utilizes each component's correlation to calculate its discriminator output, thus avoiding the influences of different navigation messages and the secondary codes modulated in components. Then, the discriminator outputs of all components are weighted combined according to levels of each component's tracking thermal noise to derive the tracking results with minimal thermal noise. Considering the bandwidths of front end, discriminator types and component powers, which determine tracking thermal noise levels, the combination weights can be optimized under the optimal thermal noise criterion, which will be introduced in detail in next subsection.

### DMT
According to the above analysis and design principles, DMT, which can both effectively utilize the high-frequency subcarriers and all the components in WMSs for carrier, subcarrier, and code tracking, can be summarized. In DMT, carrier tracking adopts two Phase Lock Loops (PLL) to track lower and upper carriers, respectively, subcarrier tracking adopts a Subcarrier Phase Lock Loop (SPLL) to track the subcarrier, and code tracking adopts a Delay Lock Loop (DLL) to track the code. More specifically, DMT calculates the lower and upper sub-band correlations for lower carrier $f_o^l$ and upper carrier $f_o^u$, respectively. Then, DMT combines the discriminator outputs of lower and upper sub-band components under the optimal thermal noise criterion to extract carrier, subcarrier and code phases of WMSs. Figure 4 exhibits the schematic of DMT, where two PLLs are labeled in green, DLL is labeled in blue, and SPLL is labeled in red. The detailed
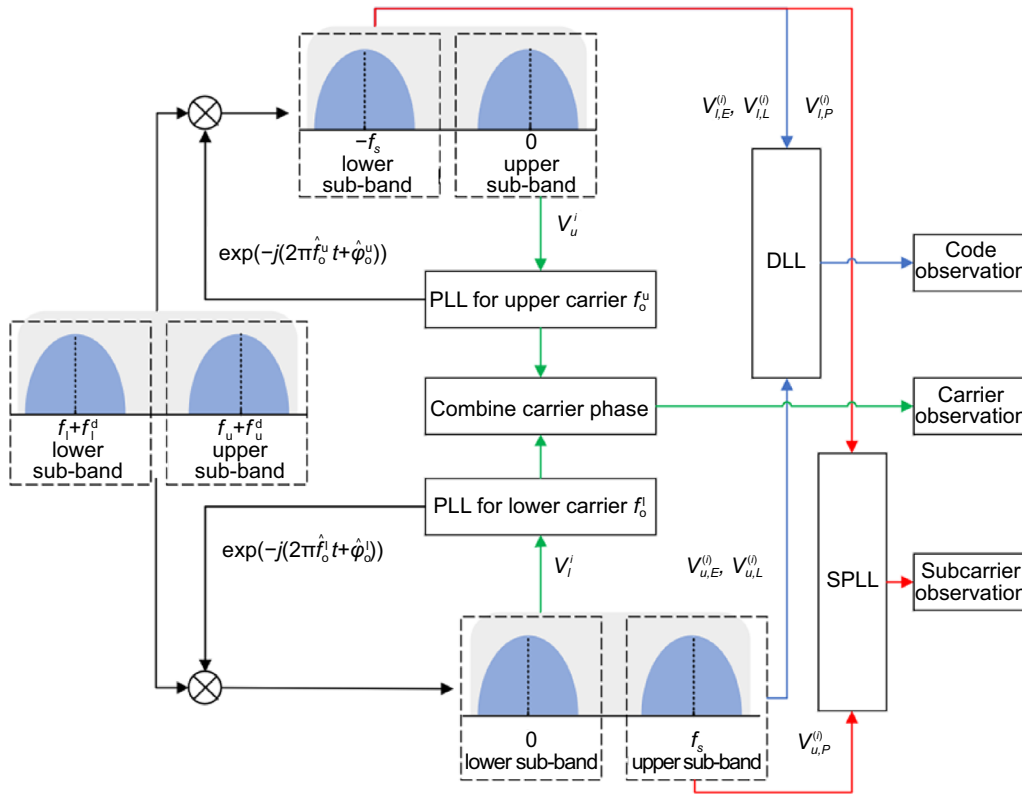
**Fig. 4** Schematic of DMT

implementation of carrier, subcarrier, and code tracking will be introduced in this subsection.

### Carrier tracking

According to the designed DMT, it has one PLL for lower carrier tracking and one PLL for upper carrier tracking. For stably tracking lower and upper carriers, lower sub-band correlation $V_l^{(i)}$ in (19) will be used to track lower carrier $f_o^l$, and upper sub-band correlation $V_u^{(i)}$ in (13) will be used to track upper carrier $f_o^u$. Since these correlations are influenced by $d_x^{(i)}$, both PLLs for lower and upper carrier tracking should adopt Costas Phase Lock Loops (CPLL). The carrier phase of WMSs will be obtained by combining the two carrier phases estimated by lower and upper carrier tracking loops, respectively.

More specifically, when lower and upper carrier frequency errors $\Delta f_o^l \approx 0$ and $\Delta f_o^u \approx 0$, the corresponding correlations can be reformed by (13) and (19) as

$$V_u^{(i)} \approx \frac{\sqrt{P_u^{(i)}}}{2} d_u^{(i)} R_u^{(i)}(\Delta \tau) \exp\left\{ j\Delta \varphi_o^u \right\} \tag{20}$$

and

$$V_l^{(i)} \approx \frac{\sqrt{P_l^{(i)}}}{2} d_l^{(i)} R_l^{(i)}(\Delta \tau) \exp\left\{ j\Delta \varphi_o^l \right\} \tag{21}$$

respectively. Therefore, for each PLL, the carrier phase error is the optimal convex combination of component's carrier discriminator outputs in the corresponding sub-band under the optimal thermal noise criterion, which can be calculated as

$$\Delta \hat{\varphi}_o^x = \sum_{i=1}^{N_x} w_{x,\text{PLL}}^{(i)} \Delta \hat{\varphi}_{o,i}^x \tag{22}$$

where $\Delta \hat{\varphi}_{o,i}^x = \operatorname{atan}\left\{ \operatorname{Im}\left( V_x^{(i)} \right) / \operatorname{Re}\left( V_x^{(i)} \right) \right\}$ is the single-component PLL discriminator output by utilizing component $r_x^{(i)}(t)$, and $w_{x,\text{PLL}}^{(i)}$ is the optimal convex combination weight, which can be optimized by

$$\min \quad \sum_{i=1}^{N_x} \left( w_{x,\mathrm{PLL}}^{(i)} \right)^2 \left( \sigma_{x,\mathrm{PLL}}^{(i)} \right)^2$$

$$\text{s.t.} \quad \sum_{i=1}^{N_x} w_{x,\mathrm{PLL}}^{(i)} = 1 \tag{23}$$

$$1 \geq w_{x,\mathrm{PLL}}^{(i)} \geq 0 \quad \forall i \in \{1 \cdots N_x\}$$

where $\sigma_{x,\mathrm{PLL}}^{(i)}$ is the tracking jitter of single-component PLL, whose values will be exhibited in detail in next section. The optimized $w_{x,\mathrm{PLL}}^{(i)}$ is

$$w_{x,\mathrm{PLL}}^{(i)} = \frac{\left( \sigma_{x,\mathrm{PLL}}^{(i)} \right)^{-2}}{\sum_{m=1}^{N_x} \left( \sigma_{x,\mathrm{PLL}}^{(m)} \right)^{-2}} \tag{24}$$

The estimated lower carrier phase error $\Delta\hat{\varphi}_o^l$ and upper carrier phase error $\Delta\hat{\varphi}_o^u$ will be separately used to track lower and upper carriers.

For carrier phases, the estimated lower carrier phase $\hat{\phi}_o^l$ and upper carrier phase $\hat{\phi}_o^u$ will also be combined in the observation domain, which is

$$\hat{\phi}_o = \frac{\hat{\phi}_o^l + \hat{\phi}_o^u}{2} \tag{25}$$

Similarly, the combination of lower and upper carrier phases in meter can be correspondingly expressed as

$$\hat{\zeta}_o = \frac{\lambda_o}{2} \left( \frac{\hat{\zeta}_o^l}{\lambda_o^l} + \frac{\hat{\zeta}_o^u}{\lambda_o^u} \right) \tag{26}$$

where $\hat{\zeta}_o^l$ and $\hat{\zeta}_o^u$ are lower and upper carrier phases in meter, $\lambda_o^l = c/f_o^l$, $\lambda_o^u = c/f_o^u$ and $\lambda_o = 2c/\left( f_o^l + f_o^u \right)$ are wavelengths of lower carrier, upper carrier, and the combined carrier, and $c$ is the speed of light.

### Code tracking

To stably track codes in WMSs, DLL should be implemented. According to the design of DMT, DLL will utilize the early and late lower sub-band correlations $V_{l,\mathrm{E}}^{(i)}$, $V_{l,\mathrm{L}}^{(i)}$ in (14) for upper carrier $f_o^u$ and the early and late upper sub-band correlations $V_{u,\mathrm{E}}^{(i)}$, $V_{u,\mathrm{L}}^{(i)}$ in (18) for lower carrier $f_o^l$. When carrier and subcarrier are tracked stably, which means that $\Delta f_o^l \approx 0$, $\Delta f_o^u \approx 0$ and $\Delta f_s \approx 0$, early and late correlations in (14) and (18) can be written as

$$V_{l,\mathrm{E}}^{(i)} \approx \frac{\sqrt{P_l^{(i)}}}{2} d_l^{(i)} R_l^{(i)}(\Delta\tau - \mu) \exp\left\{ \mathrm{j}\left( \Delta\varphi_o^u - \Delta\varphi_s \right) \right\}$$

$$V_{l,\mathrm{L}}^{(i)} \approx \frac{\sqrt{P_l^{(i)}}}{2} d_l^{(i)} R_l^{(i)}(\Delta\tau + \mu) \exp\left\{ \mathrm{j}\left( \Delta\varphi_o^u - \Delta\varphi_s \right) \right\} \tag{27}$$

and

$$V_{u,\mathrm{E}}^{(i)} \approx \frac{\sqrt{P_u^{(i)}}}{2} d_u^{(i)} R_u^{(i)}(\Delta\tau - \mu) \exp\left\{ \mathrm{j}\left( \Delta\varphi_o^l + \Delta\varphi_s \right) \right\}$$

$$V_{u,\mathrm{L}}^{(i)} \approx \frac{\sqrt{P_u^{(i)}}}{2} d_u^{(i)} R_u^{(i)}(\Delta\tau + \mu) \exp\left\{ \mathrm{j}\left( \Delta\varphi_o^l + \Delta\varphi_s \right) \right\} \tag{28}$$

respectively. Under the optimal thermal noise criterion, the discriminator output of DLL is the optimal convex combination of component's code discriminator outputs, which can be calculated as

$$\Delta\hat{\tau} = \sum_{x \in \{u,l\}} \sum_{i=1}^{N_x} w_{x,\mathrm{DLL}}^{(i)} \Delta\hat{\tau}_x^{(i)} \tag{29}$$

where $\Delta\hat{\tau}_x^{(i)}$ is the single-component DLL's discriminator output by utilizing component $r_x^{(i)}(t)$. Code discriminators have two modes, which are coherent and non-coherent discriminators. For coherent code discriminators, $\Delta\hat{\tau}_x^{(i)}$ can be calculated by

$$\Delta\hat{\tau}_x^{(i)} = \mathrm{Re}\left\{ V_{x,\mathrm{E}}^{(i)} \right\} - \mathrm{Re}\left\{ V_{x,\mathrm{L}}^{(i)} \right\} \tag{30}$$

For non-coherent code discriminators, $\Delta\hat{\tau}_x^{(i)}$ can be calculated by

$$\Delta\hat{\tau}_x^{(i)} = \left\| V_{x,\mathrm{E}}^{(i)} \right\|^2 - \left\| V_{x,\mathrm{L}}^{(i)} \right\|^2 \tag{31}$$

where $\|y\|$ is the norm of $y$. The optimal convex combination weights $w_{x,\mathrm{DLL}}^{(i)}$ used in (29) can be optimized by

$$\min \quad \sum_{x \in \{u,l\}} \sum_{i=1}^{N_x} \left( w_{x,\mathrm{DLL}}^{(i)} \right)^2 \left( \sigma_{x,\mathrm{DLL}}^{(i)} \right)^2$$

$$\text{s.t.} \quad \sum_{x \in \{u,l\}} \sum_{i=1}^{N_x} w_{x,\mathrm{DLL}}^{(i)} = 1$$

$$1 \geq w_{x,\mathrm{DLL}}^{(i)} \geq 0 \quad \forall i \in \{1 \cdots N_x\}, \forall x \in \{u,l\} \tag{32}$$

Qi *et al. Satellite Navigation*      (2024) 5:5

Page 12 of 22

where $\sigma_{x,\text{DLL}}^{(i)}$ is the tracking jitter of single-component DLL. $w_{x,\text{DLL}}^{(i)}$ optimized by (32) is

$$w_{x,\text{DLL}}^{(i)} = \frac{\left(\sigma_{x,\text{DLL}}^{(i)}\right)^{-2}}{\sum\limits_{m\in\{u,l\}}\sum\limits_{n=1}^{N_m}\left(\sigma_{m,\text{DLL}}^{(n)}\right)^{-2}} \tag{33}$$

The estimated $\Delta\hat{\tau}$ will be used to update the local codes to stably track codes in WMSs. Since the codes tracked by code tracking loop are not modulated by the subcarriers with frequency $f_s$, the estimated code phase $\hat{\tau}_c$ should be unambiguous but low precision.

### Subcarrier tracking

Unlike carrier tracking, DMT only needs one SPLL so that all the components in lower and upper sub-bands can be involved. Since the correlations of components are influenced by $d_x^{(i)}$, SPLL should also adopt CPLL. SPLL in DMT utilizes the prompt lower sub-band correlation $V_{l,\text{P}}^{(i)}$ for upper carrier $f_o^u$ in (14) and prompt upper sub-band correlation $V_{u,\text{P}}^{(i)}$ for lower carrier $f_o^l$ in (18). When carriers are stably tracked and the subcarrier frequency is properly estimated, which means that $\Delta f_o^l$, $\Delta f_o^u$, $\Delta\varphi_o^l$, $\Delta\varphi_o^u$ and $\Delta f_s$ take the value of zero, correlations $V_{u,\text{P}}^{(i)}$ and $V_{l,\text{P}}^{(i)}$ can be further reformed as

$$V_{u,\text{P}}^{(i)} \approx \frac{\sqrt{P_u^{(i)}}}{2} d_u^{(i)} R_u^{(i)}(\Delta\tau)\exp\left\{\text{j}(+\Delta\varphi_s)\right\} \tag{34}$$

and

$$V_{l,\text{P}}^{(i)} \approx \frac{\sqrt{P_l^{(i)}}}{2} d_l^{(i)} R_l^{(i)}(\Delta\tau)\exp\left\{\text{j}(-\Delta\varphi_s)\right\} \tag{35}$$

respectively. Therefore, under the optimal thermal noise criterion, the subcarrier phase error $\Delta\hat{\varphi}_s$ is the optimal convex combination of component's subcarrier discriminator outputs, which can be expressed as

$$\Delta\hat{\varphi}_s = \sum_{x\in\{u,l\}}\sum_{i=1}^{N_x} w_{x,\text{SPLL}}^{(i)}\gamma^x\Delta\hat{\varphi}_{s,i}^x \tag{36}$$

where $\Delta\hat{\varphi}_{s,i}^x = \text{atan}\left\{\text{Im}\left(V_{x,P}^{(i)}\right)/\text{Re}\left(V_{x,P}^{(i)}\right)\right\}$ is the single-component SPLL discriminator output, $\gamma^x$ takes the value of 1 when $x = u$ and the value of $-1$ when $x = l$, and $w_{x,\text{SPLL}}^{(i)}$ can be optimized by

$$\min \quad \sum_{x\in\{u,l\}}\sum_{i=1}^{N_x}\left(w_{x,\text{SPLL}}^{(i)}\right)^2\left(\sigma_{x,\text{SPLL}}^{(i)}\right)^2$$

$$\text{s.t.} \quad \sum_{x\in\{u,l\}}\sum_{i=1}^{N_x} w_{x,\text{SPLL}}^{(i)} = 1$$

$$1 \geq w_{x,\text{SPLL}}^{(i)} \geq 0 \quad \forall i \in \{1\cdots N_x\}, \forall x \in \{u,l\} \tag{37}$$

where $\sigma_{x,\text{SPLL}}^{(i)}$ is the tracking jitter of single-component SPLL. The optimized $w_{x,\text{SPLL}}^{(i)}$ is

$$w_{x,\text{SPLL}}^{(i)} = \frac{\left(\sigma_{x,\text{SPLL}}^{(i)}\right)^{-2}}{\sum\limits_{m\in\{u,l\}}\sum\limits_{n=1}^{N_m}\left(\sigma_{m,\text{SPLL}}^{(n)}\right)^{-2}} \tag{38}$$

The subcarrier phase error $\Delta\hat{\varphi}_s$ estimated by (36) will be used for subcarrier tracking. Since CPLL is implemented in SPLL, the estimated subcarrier phase $\hat{\tau}_s$ may deviate by an integer multiplying half a subcarrier period, which can be denoted as $N_s T_s$, where $N_s \in \mathbb{Z}$ and $T_s = 1/2f_s$. Therefore, the subcarrier phases estimated by subcarrier tracking loops are high precision but ambiguous. To obtain the unambiguous subcarrier phases, DMT adopts the methods proposed in (Hameed et al., 2021; Qi et al., 2022; 2023; Wendel et al., 2014) which solve subcarrier ambiguity $N_s$ in position domain, and thus repairing subcarrier ambiguities.

### Implementation of DMT

Figure 5 exhibits the detailed tracking structures of DMT. In Fig. 5, two PLLs are labeled in green, SPLL is labeled in red, and DLL is labeled in blue. According to the detailed DMT in Fig. 5, DMT utilizes both lower and upper sub-band components of WMSs in carrier, subcarrier, and code tracking, which means that the estimated carrier, subcarrier, and code phases have higher precision. It should be noted that DMT utilizes the high precision and unambiguous subcarrier phases $\hat{\tau}_s$. Therefore, the ranging precision of DMT is determined by estimated subcarrier phases.

Since DMT utilizes all the components in WMSs in tracking, more correlations should be calculated in DMT compared with other tracking methods. Therefore, DMT requires more computation resources. More specifically, the required computation resources are directly related
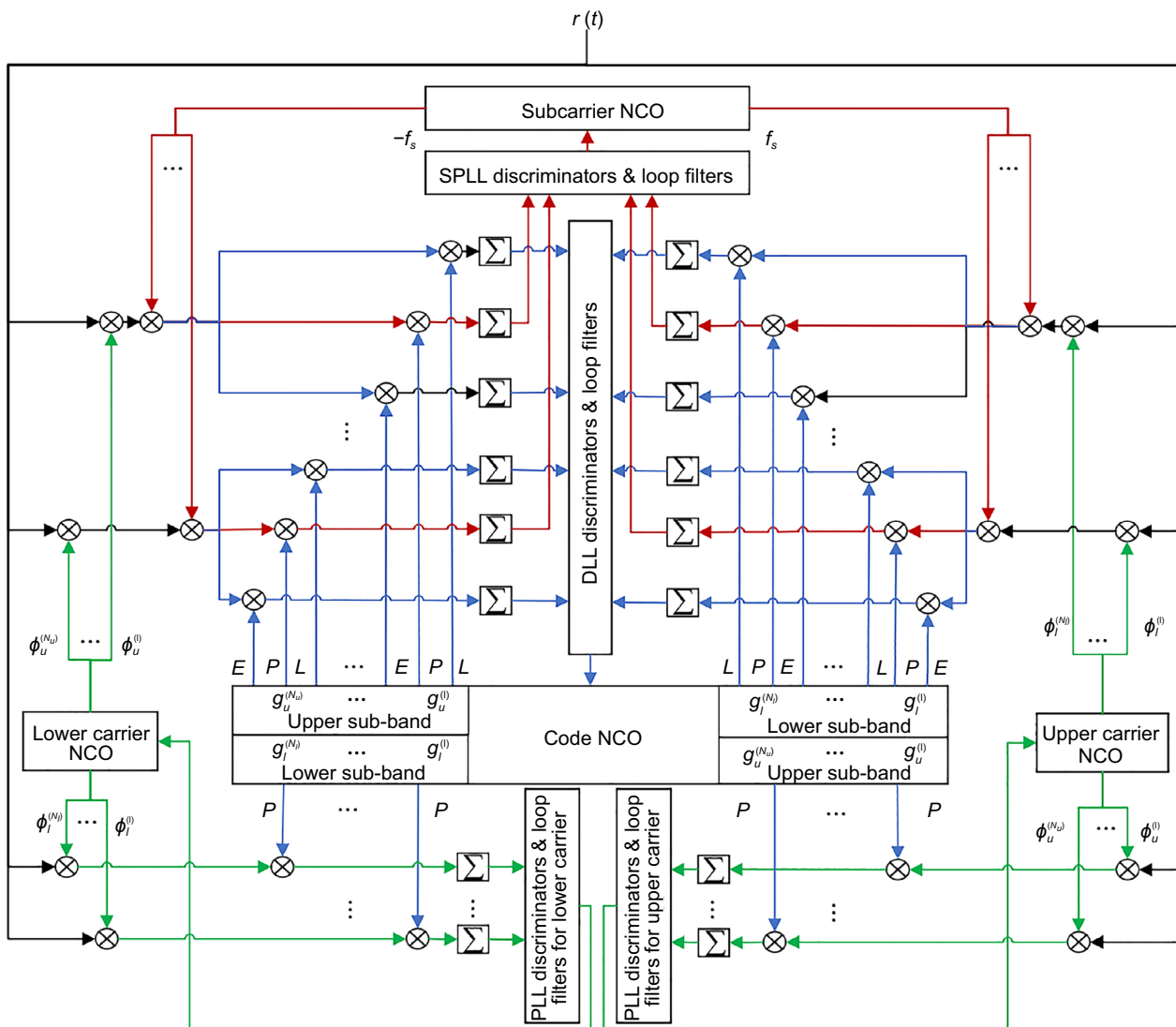
**Fig. 5** Detailed tracking structure of DMT

**Table 2** Required numbers of complex correlators in carrier, subcarrier and code tracking of different tracking methods

| Methods | Complex correlator number | | |
|---|---|---|---|
| | PLL | SPLL | DLL |
| Symmetric tracking method | 2 | 2 | 2 |
| Asymmetric tracking method | 1 | 1 | 1 |
| DMT | $N_l + N_u$ | $N_l + N_u$ | $2(N_l + N_u)$ |

**Table 3** Approximated theoretical tracking jitters of CAT, DBT and DMT methods in carrier, subcarrier, coherent code and non-coherent code tracking loops

| Methods | PLL | SPLL | Coherent DLL | Non-coherent DLL |
|---|---|---|---|---|
| CAT | $R\sigma_o$ | $2R\sigma_s$ | $R\sigma_{c,\mathrm{coh}}$ | $R\sigma_{c,\mathrm{noncoh}}$ |
| DBT | $\frac{R}{\sqrt{2}}\sigma_o$ | $\sqrt{2}R\sigma_s$ | $\frac{R}{\sqrt{2}}\sigma_{c,\mathrm{coh}}$ | $\frac{R}{\sqrt{2}}\sigma_{c,\mathrm{noncoh}}$ |
| DMT | $\sigma_o$ | $\sigma_s$ | $\sigma_{c,\mathrm{coh}}$ | $\sigma_{c,\mathrm{noncoh}}$ |

Qi *et al. Satellite Navigation* (2024) 5:5

Page 14 of 22

to the numbers of complex correlators. For carrier tracking, there are two PLLs in DMT, thus the required number of complex correlators is $N_l + N_u$. For subcarrier tracking, DMT utilizes the prompt correlations from lower and upper sub-bands, thus the required number of complex correlators in subcarrier tracking is also $N_l + N_u$. For code tracking, DMT utilizes the early and late correlations of both lower and upper sub-bands, thus $2(N_l + N_u)$ complex correlators are required in code tracking. Table 2 lists the complex correlator numbers required in carrier, subcarrier, and code tracking for the symmetric tracking method, asymmetric tracking method and DMT. Compared with other techniques, although DMT requires more computation resources, its higher computational demands can be fulfilled as the rapid development of high-performance computing equipment.

## Performance analysis

To comprehensively assess the tracking and ranging performances of DMT, this section first derives the theoretical tracking jitters of carrier, subcarrier and code tracking in DMT. Then, simulation and real experiments are conducted to further verify the effectiveness of DMT.

For fairly evaluating DMT's performance, a symmetric subcarrier method, that is the DBT method and an asymmetric subcarrier method, that is the CAT method, are implemented as baselines to further compare with DMT in theoretical analysis, simulation, and real experiments.

### Theoretical analysis

According to classic tracking loop theory in (Betz & Kolodziejski, 2009a; b; Borio, 2014; Julien, 2005; Tran, 2004; Tran & Hegarty, 2002), denoting the filter bandwidths used in the carrier, subcarrier, and code tracking as the $B_n^{\text{PLL}}$,

$B_n^{\text{SPLL}}$ and $B_n^{\text{DLL}}$, the theoretical tracking jitters of carrier, subcarrier, coherent code, and non-coherent code tracking loops can be expressed as (48), (54), (60) and (61) respectively, and their detailed derivations are in Appendix A.

When the carrier wavelengths, modulations, and component powers of lower and upper sub-bands are similar, theoretical carrier tracking jitter $\sigma_o$, subcarrier tracking jitter $\sigma_s$, coherent code tracking jitter $\sigma_{c,\text{coh}}$ and non-coherent code tracking jitter $\sigma_{c,\text{noncoh}}$ can be approximated as

$$\sigma_o \approx \frac{\lambda_o^x}{2\pi} \sqrt{\frac{B_n^{\text{PLL}}\left(1 - 0.5 B_n^{\text{PLL}} T\right)}{(N_l + N_u) P_x^{(i)}/N_0} \left[1 + \frac{1}{2 T P_x^{(i)}/N_0}\right]}$$
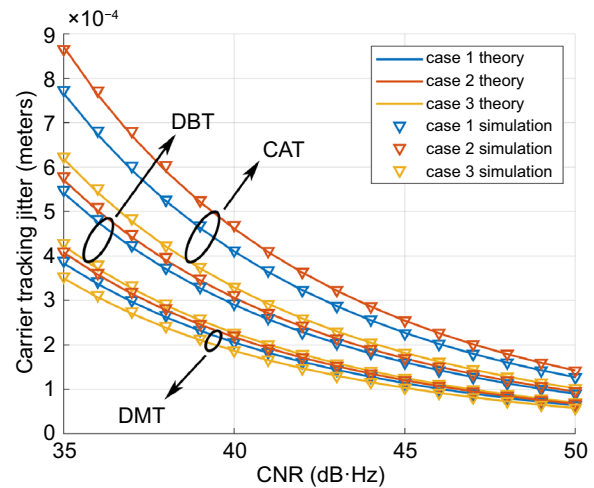
(39)



**Fig. 6** Carrier tracking jitters of CAT, DBT and DMT for three different cases

**Table 4** Specific settings of three different WMS cases and theoretical tracking jitter improvements

| Cases | Sub-bands | $N_x$ | $f_x$ (MHz) | $g_x^{(i)}$ | $d_x^{(i)}$ | Modulation | $\phi_x^{(i)}(°)$ | $P_x^{(i)}$ ratio | $\delta_o^{\text{CAT}}/\delta_o^{\text{DBT}}$ | $\delta_s^{\text{CAT}}/\delta_s^{\text{DBT}}$ | $\delta_c^{\text{CAT}}/\delta_c^{\text{DBT}}$ |
|---|---|---|---|---|---|---|---|---|---|---|---|
| Case 1 | Lower | 2 | 1176.45 | $g_l^{(1)}$ | −1 | BPSK(10) | 0 | 1 | 50.0%/29.3% | 50.0%/64.6% | 50.0%/29.3% |
| | | | 1176.45 | $g_l^{(2)}$ | 1 | BPSK(10) | 90 | 1 | | | |
| | Upper | 2 | 1207.14 | $g_u^{(1)}$ | 1 | BPSK(10) | 0 | 1 | | | |
| | | | 1207.14 | $g_u^{(2)}$ | −1 | BPSK(10) | 90 | 1 | | | |
| Case 2 | Lower | 2 | 1176.45 | $g_l^{(1)}$ | −1 | BPSK(10) | 0 | 1 | 53.0%/28.9% | 47.0%/64.5% | 47.3%/29.2% |
| | | | 1176.45 | $g_l^{(2)}$ | 1 | BPSK(10) | 90 | 1 | | | |
| | Upper | 2 | 1207.14 | $g_u^{(1)}$ | 1 | BPSK(10) | 0 | 0.8 | | | |
| | | | 1207.14 | $g_u^{(2)}$ | −1 | BPSK(10) | 90 | 0.8 | | | |
| Case 3 | Lower | 1 | 1561.098 | $g_l^{(1)}$ | 1 | BPSK(2) | 0 | 1 | 43.4%/17.4% | 40.0%/58.7% | 48.0%/20.3% |
| | Upper | 2 | 1575.42 | $g_u^{(1)}$ | 1 | BOC(1,1) | 0 | 0.9 | | | |
| | | | 1575.42 | $g_u^{(2)}$ | −1 | BOC(1,1) | 90 | 0.9 | | | |

Qi *et al. Satellite Navigation*          (2024) 5:5

Page 15 of 22

$$\sigma_s \approx \frac{\lambda_s}{2\pi} \sqrt{\frac{B_n^{\mathrm{SPLL}}\left(1 - 0.5B_n^{\mathrm{SPLL}}T\right)}{(N_l + N_u)P_x^{(i)}/N_0}\left[1 + \frac{1}{2TP_x^{(i)}/N_0}\right]} \tag{40}$$

$$\sigma_{c,\mathrm{coh}} \approx c\sqrt{\frac{k_{x,1}^{(i)}B_n^{\mathrm{DLL}}\left(1 - 0.5B_n^{\mathrm{DLL}}T\right)}{4\pi^2 k_{x,2}^{(i)}(N_l + N_u)P_x^{(i)}/N_0}} \tag{41}$$

$$\sigma_{c,\mathrm{noncoh}} \approx c\sqrt{\frac{k_{x,1}^{(i)}B_n^{\mathrm{DLL}}\left(1 - 0.5B_n^{\mathrm{DLL}}T\right)}{4\pi^2 k_{x,2}^{(i)}(N_l + N_u)P_x^{(i)}/N_0}\left[1 + \frac{k_{x,3}^{(i)}}{Tk_{x,4}^{(i)}P_x^{(i)}/N_0}\right]} \tag{42}$$

respectively, where $\lambda_s = c/f_s$ is the subcarrier wavelength, and $k_{x,1}^{(i)}$, $k_{x,2}^{(i)}$, $k_{x,3}^{(i)}$, $k_{x,4}^{(i)}$ are referred to (59).

Table 3 exhibits the approximated theoretical tracking jitters of CAT, DBT, and DMT methods in carrier, subcarrier, coherent code, and non-coherent code tracking loops, where $R = \sqrt{N_l + N_u}$. Since CAT and DBT utilizes one component and two components in carrier tracking, respectively, the carrier tracking jitter improvement of DMT is $\delta_o^{\mathrm{CAT}} = 1 - 1/R$ with respect to CAT, and $\delta_o^{\mathrm{DBT}} = 1 - \sqrt{2}/R$ with respect to DBT. Since the subcarrier tracking in CAT only utilizes one component in lower sub-band, and the used subcarrier wavelength is $\lambda_s$, its subcarrier tracking jitter improvement of DMT is $\delta_s^{\mathrm{CAT}} = 1 - 1/(2R)$ with respect to CAT. While the subcarrier tracking in DBT utilizes two components and the used subcarrier wavelength is $2\lambda_s$, therefore its subcarrier tracking jitter improvement of DMT is $\delta_s^{\mathrm{DBT}} = 1 - 1/\left(\sqrt{2}R\right)$ with respect to DBT. Because the CAT utilizes one component and DBT utilizes two components in code tracking, the coherent and non-coherent code tracking jitter improvements of DMT are
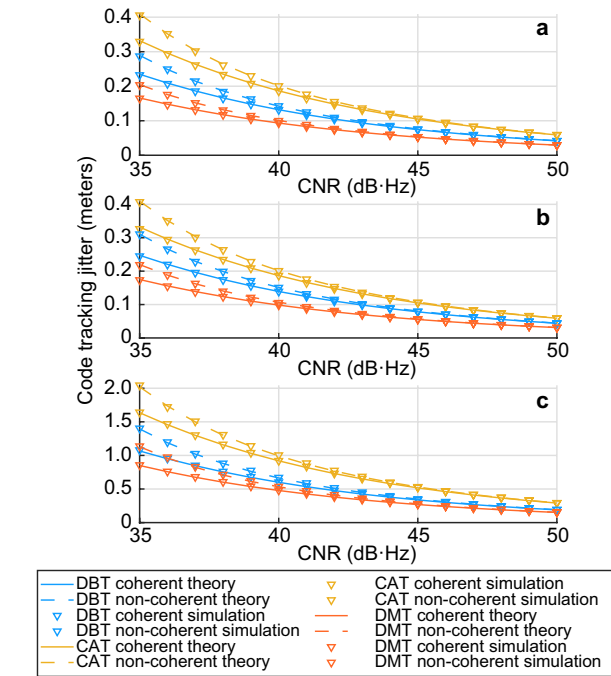


**Fig. 8** Coherent and non-coherent code tracking jitters of CAT, DBT and DMT for **a** Case 1, **b** Case 2 and **c** Case 3

$\delta_c^{\mathrm{CAT}} = 1 - 1/R$ with respect to CAT, and $\delta_c^{\mathrm{DBT}} = 1 - \sqrt{2}/R$ with respect to DBT.

## Simulation experiments

To analyze the carrier, subcarrier, and code tracking performances of DMT, Monte Carlo (MC) based simulation experiments for three different WMS cases are implemented under different carrier to noise ratios (CNR). The detailed settings of three WMS cases and theoretical tracking jitter improvements are exhibited in Table 4. The optimal convex combination weights used in the carrier, subcarrier, and code tracking of DMT are calculated accordingly by (24), (38) and (33), which will not be detailed in this paper. The theoretical tracking jitters are also exhibited in this subsection to cross verify with the simulated results. The filter bandwidths used in carrier, subcarrier, and code tracking are 2 Hz, 1 Hz and 1 Hz, respectively, and pre-correlation time is 1 ms.

Figure 6 exhibits the theoretical and simulated carrier tracking jitters of CAT, DBT, and DMT for three cases. The coincidence between the theoretical and simulated results indicate the correctness of theory derivations and simulation experiments. Since Case 3 has higher carrier frequencies than Case 1 and Case 2, the carrier tracking jitters of Case 3 should be lower than those of Case 1 and Case 2 for each method. As Fig. 6 shows, for each case the carrier tracking jitter of DMT is smaller than that of CAT and DBT, which means that the multiple components in
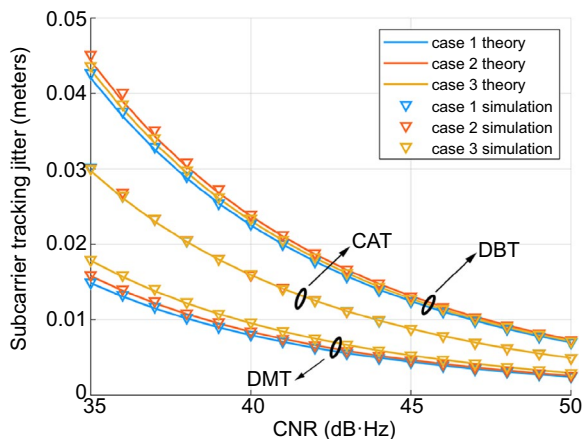


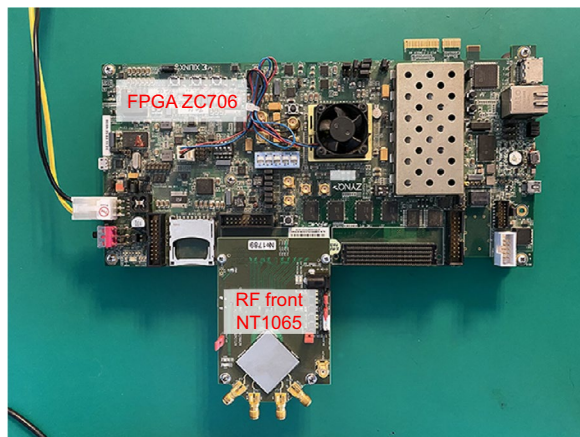**Fig. 7** Subcarrier tracking jitters of CAT, DBT and DMT for three different cases

Qi *et al. Satellite Navigation* (2024) 5:5

Page 16 of 22



**Fig. 9** Data collection location



**Fig. 10** Multi-system multi-band GNSS raw data collector

**Table 5** Tracking settings for CAT, DBT and DMT

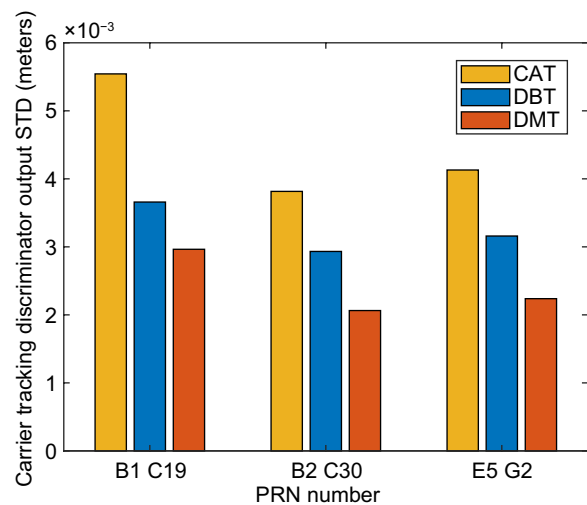| Parameters | Values |
| --- | --- |
| PLL order | 2 |
| PLL bandwidth $\left(B_n^{PLL}\right)$ | 2 Hz |
| SPLL order | 2 |
| SPLL bandwidth $\left(B_n^{SPLL}\right)$ | 5 Hz |
| DLL order | 2 |
| DLL bandwidth $\left(B_n^{DLL}\right)$ | 5 Hz |
| DLL early/late code phase delay $(\pm\mu)$ | $\pm 0.5$ code chip |
| Pre-correlation time $(T)$ | 1 ms |



**Fig. 11** Carrier tracking discriminator outputs STDs of CAT, DBT and DMT for three WMSs

WMSs are effectively utilized by DMT. For Case 1, compared with CAT and DBT, the carrier tracking jitters of DMT are improved by 50.2% and 29.2%. Since Case 1 is an equal component power case while Case 2 is the unequal component power case, CAT, DBT, and DMT's carrier tracking jitters of Case 2 should be slightly higher than that of Case 1. For Case 2, the carrier tracking jitters of DMT are improved by 53.2% and 29% compared with CAT and DBT. Since Case 3 has only three components in Case 3, the carrier tracking jitter of DMT is obviously higher than those for Case 1 and Case 2. Compared with CAT and DBT, DMT's carrier tracking jitter in Case 3 is improved by 43.3% and 17.6%, respectively.

Figure 7 exhibits the subcarrier tracking jitters of CAT, DBT, and DMT for three different cases. As Fig. 7 shows, DMT's subcarrier tracking jitters in all cases are lower than CAT and DBT. Since CAT utilizes one component $g_l^{(1)}(t)$ in lower sub-band to tracking subcarrier, and the lower sub-band components $g_l^{(1)}(t)$ for three cases have the same powers, their subcarrier tracking jitters of CAT should be nearly the same.

Compared with CAT, although the subcarriers tracked by CAT and DMT have the same frequencies, DMT utilizes more components in subcarrier tracking, thus have lower subcarrier tracking jitters. For three cases, the subcarrier tracking jitters of DMT are improved by 49.9%, 46.8% and 39.8%, respectively compared with CAT. Compared with DBT, the subcarrier tracked by DMT has the higher frequency and more components are effectively used by DMT, it therefore has lower subcarrier tracking jitters, which are improved by 64.4%, 64.5% and 58.6% for three cases.

Figure 8a−c exhibits the CAT, DBT and DMT's coherent and non-coherent code tracking jitters for three cases. As Fig. 8 shows, when CNR is high, non-coherent code tracking jitters are similar to coherent code tracking jitters. When CNR is low, since the square losses of non-coherent discriminators cannot be ignored, non-coherent code tracking jitters are obviously higher than that of coherent code tracking jitters, which is consistent with the conclusions in
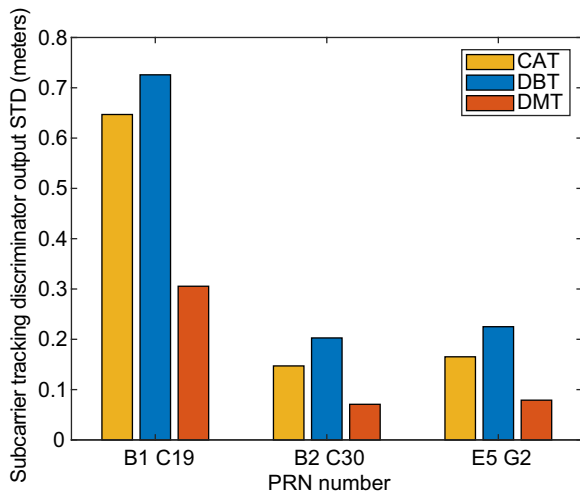
**Fig. 12** Subcarrier tracking discriminator outputs STDs of CAT, DBT and DMT for three WMSs
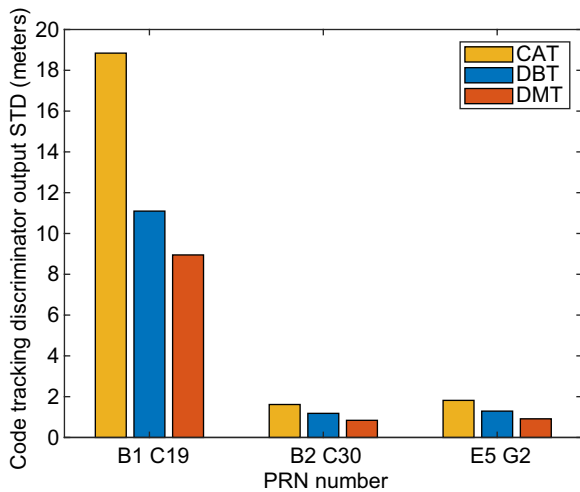


**Fig. 13** Code tracking discriminator output STDs of CAT, DBT and DMT for three WMSs

(Betz & Kolodziejski, 2009a; b). According to Table 4, the components in Case 1 and Case 2 adopt the BPSK(10) modulations while the components in Case 3 adopt the BPSK(2) or BOC(1,1) modulations, whose code chip lengths are longer than BPSK(10), thus the code tracking jitters of Case 3 are obviously higher than those of Case 1 and Case 2. In all three cases, DMT still has lowest code tracking jitters among three methods. Compared with CAT, the code tracking jitters of DMT are improved by 50.1%, 47.4% and 48.2%. When compared with DBT, the code tracking jitters of DMT are improved by 29.3%, 29.5% and 20.2%. It should be noted that CAT in Case 2 uses a lower sub-band component which has an identical ACF with upper sub-band component, while CAT in Case 3 uses a lower sub-band component which has a flatter ACF peak than upper sub-band components, so even though DMT in Case 3 uses one less components than in Case 2, the DMT's code tracking jitter improvement of Case 3 is still similar to that of Case 2.

The consistence between theoretical and simulated results reveal that the theoretical derivations and simulation experiments are correct. Through the analysis of the results from different cases and methods, DMT has lower carrier, subcarrier, and code tracking jitters than CAT and DBT, implying the effectiveness and superiority of DMT in utilizing the high precision tracking and ranging potential of WMSs.

## Real experiments

To verify the effectiveness of DMT in real environments, three real experiments for E5 WMS, B1 WMS, and B2 WMS were conducted. The raw data were recorded on the roof of Weiqing Building of Tsinghua University in Beijing, which is exhibited in Fig. 9. The raw data collector is a multi-system multi-band GNSS data collectors exhibited in Fig. 10. The data for E5 WMS and B2 WMS were recorded around 11:44 am (UTC+8) on June 5, 2022

**Table 6** Code, subcarrier, and code tracking jitter improvements of DMT with respect to CAT and DMT in theoretical and real data experiments

| Signal | Theoretical (%) | | | | | | Real data (%) | | | | | |
|---|---|---|---|---|---|---|---|---|---|---|---|---|
| | $\sigma_o^{CAT}$ | $\sigma_o^{DBT}$ | $\sigma_s^{CAT}$ | $\sigma_s^{DBT}$ | $\sigma_c^{CAT}$ | $\sigma_c^{DBT}$ | $\sigma_o^{CAT}$ | $\sigma_o^{DBT}$ | $\sigma_s^{CAT}$ | $\sigma_s^{DBT}$ | $\sigma_c^{CAT}$ | $\sigma_c^{DBT}$ |
| B1 WMS | 43.4 | 17.4 | 40.0 | 58.7 | 48.0 | 20.3 | 46.5 | 19.0 | 52.8 | 57.9 | 52.5 | 19.4 |
| B2 WMS | 53.0 | 28.9 | 47.0 | 64.6 | 47.3 | 29.2 | 45.9 | 29.6 | 51.9 | 65.1 | 48.0 | 28.9 |
| E5 WMS | 50.0 | 29.3 | 50.0 | 64.6 | 50.0 | 29.3 | 45.8 | 29.2 | 52.2 | 64.9 | 49.7 | 29.2 |

and the data for B1 WMS were recorded around 6:20 pm (UTC+8) on June 27, 2022.

In the experiments, the results include not only the discriminator outputs in carrier, subcarrier, and code tracking loops to evaluate the tracking performances, but also the Pseudorange Minus Carrier (PMC) results to assess the ranging performances. B1 WMS broadcast by BDS-3 C19 satellite, B2 WMS broadcast by BDS-3 C30 satellite, and E5 WMS broadcast by Galileo G2 satellite, were separately processed, whose CNRs are around 45 dB·Hz, 49 dB·Hz and 48 dB·Hz respectively. Like the simulation experiments, DBT and CAT were also implemented to compare them with DMT. Table 5 exhibits the tracking settings used in CAT, DBT and DMT.

Figures 11, 12 and 13 exhibits the Standard Deviations (STD) of the carrier, subcarrier, and code tracking discriminator outputs of CAT, DBT and DMT for three WMSs. As figures show, when stably tracking DMT has the smallest discriminator output STDs in carrier, subcarrier, and code tracking, indicating that the DMT can more effectively take advantage of WMSs for higher precision tracking.

More specifically, for carrier tracking since CAT only uses one component while DBT uses two components, the STDs of carrier discriminator outputs of DBT should be smaller than those of CAT. Because DMT utilizes all the components in both lower and upper sub-bands, it has the smallest STDs of carrier discriminator outputs for B1 WMS, B2 WMS, and E5 WMS, indicating the higher precision carrier tracking in DMT. Compared with CAT and DBT, the STDs of DMT's carrier discriminator outputs of B2 WMS and E5 WMS are degraded by 45.9% and 29.6%, respectively, and those of DMT's carrier discriminator outputs of B1 WMS are degraded by 46.5% and 19.0%, respectively.

For subcarrier tracking, since the frequency difference between the lower and upper sub-bands of B1 WMS is 14.322 MHz while that of B2 WMS and E5 WMS is 30.69 MHz, the STDs of the subcarrier discriminator outputs of B1 WMSs are obviously larger than that of B2 WMS and E5 WMS. Although CAT only utilizes one component for subcarrier tracking which is less than the number of components used in DBT, the subcarrier frequency tracked by CAT is twice that tracked by DBT. Therefore, considering the subcarrier wavelengths and multiple components, the STDs of subcarrier discriminator outputs of CAT are slightly smaller than that of DBT. For these three different signals, DMT always has the smallest subcarrier discriminator output STDs, indicating that DMT can track subcarrier with a higher precision. Specifically, for B2 WMS and E5 WMS, the STDs of DMT's subcarrier discriminator outputs are degraded by 51.9% and 65.8%, respectively, compared with CAT and DBT. For B1 WMS, compared with CAT and DBT, the STDs of DMT's subcarrier discriminator outputs are degraded by 52.8% and 57.9%, respectively.

For code tracking, since the lower and upper sub-band components in B1 WMS adopt BPSK(2) or BOC(1,1) modulation, whose code chip lengths is much longer than that of BPSK(10) modulation adopted in components of B2 WMS and E5 WMS, the STDs of the code discriminator outputs of B1 WMS are obviously larger than those of B2 WMS or E5 WMS. For three WMSs, DMT always has the smallest STDs of the code discriminator outputs, thus the code phases extracted by DMT have higher precision. Specifically, compared with CAT, the STDs of DMT's code discriminator outputs of B2 WMS, E5 WMS and B1 WMS are decreased by 48.3%, 49.7%, and 52.5%, respectively. Compared with DBT, the STDs of DMT's code discriminator outputs of B2 WMS, E5 WMS, and B1 WMS are decreased by 28.9%, 29.2%, and 19.4%, respectively.

To intuitively evaluate the performance of DMT in the real experiments, Table 6 exhibits the code, subcarrier, and code tracking jitter improvements of DMT with respect to CAT and DMT in theoretical analysis and real experiments. As Table 6 shows, the theoretical improvements are consistent with the improvements in the real experiments, showing the correctness of theoretical analysis and real experiment results. In addition, DMT
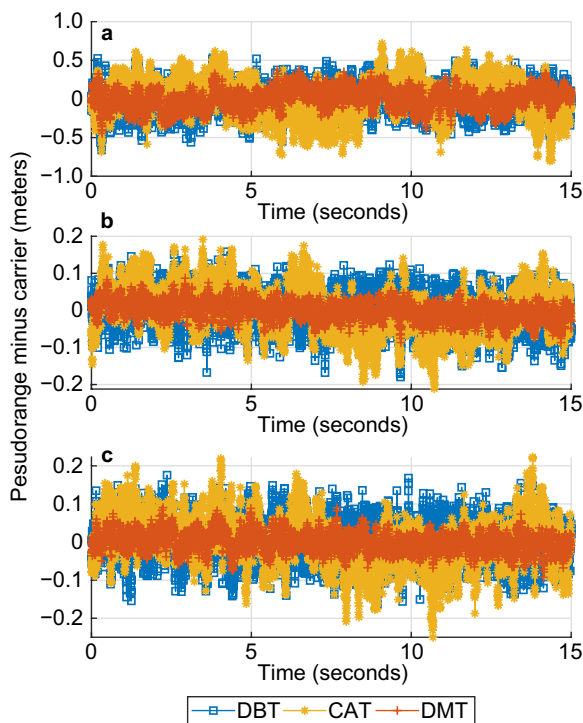


**Fig. 14** PMCs derived by CAT, DBT and DMT for **a** B1 WMS, **b** B2 WMS and **c** E5 WMS

has much better tracking performance than both CAT and DBT in carrier, subcarrier, and code tracking, indicating the effectiveness of DMT in WMS's high-precision tracking.

According to the designed DMT, the ranging precision of DMT is determined by unambiguous subcarrier phases. Therefore, Fig. 14 exhibits the PMC calculated by the subcarrier phases estimated by DMT, which reflects the pesudorange's precision without the influence of relative motions between satellite and receiver. Figure 14 also exhibits the PMC results of CAT and DBT compared with DMT. As Fig. 14 shows, the precision of CAT's PMC is slightly better than that of DBT's PMC, which are consistent with the STDs of similar subcarrier discriminator outputs of these two methods. For DMT, it can be easily observed that the PMC of DMT has the highest precision for each WMS, further verifying the ability of DMT to derive higher precision ranging results by utilizing different WMSs.

According to the STDs of discriminator outputs and PMC results exhibited above for different WMSs and different tracking methods, DMT always has better tracking and ranging performances than other methods. DMT can be effectively implemented in each WMS broadcast in next generation GNSS. Moreover, DMT can take full advantages of high-frequency subcarrier and multiple components in WMSs for higher precision tracking and ranging.

## Conclusion

The work and contributions of this paper are concluded in three aspects as below:

First, this paper developed a theoretical analysis method for WMS tracking with arbitrary local carrier by specifically designing an extended RMSB for equivalent baseband WMS. Based on this, from the perspective of CRLB, this paper also optimizes the WMS tracking structure by considering both multi-component and spectrum separation characteristics.

Second, to take full advantage of WMS for high precision tracking and ranging, this paper proposed a DMT technique. On one hand, DMT specifically designs a dual-assisted tracking structure, which not only fully use spectrum separation characteristics of WMSs but also all the components from both lower and upper sub-band for joint tracking. On the other hand, DMT specifically designs a multi-component joint tracking under the optimal thermal noise criterion to fully use the powers of all components.

Third, this paper comprehensively analyzed DMT. The theoretical carrier, subcarrier, and code tracking jitters of

DMT were derived in detail. And abundant simulation and real experiments were also implemented. According to theoretical analysis, simulation, and real experiments, DMT can derive the tracking outputs with lower jitters and ranging results with higher precision compared with existing WMS tracking methods, comprehensively revealing the effectiveness and superiority of DMT for utilizing WMSs.

DMT proposed in this paper provides not only the significant insights for exploring high precision tracking and ranging potential of next generation GNSS signals, but also the references for new generation GNSS signal designs. In the future, the effects of ionospheric delays on WMS's tracking and ranging will be further analyzed.

## Appendix: Derivation of DMT's theoretical tracking jitters

### Carrier tracking jitter

According to (23), the theoretical tracking jitter of the PLL for lower carrier or upper carrier is

$$\sigma_{x,\text{PLL}} = \sqrt{\sum_{i=1}^{N_x} \left(w_{x,\text{PLL}}^{(i)}\right)^2 \left(\sigma_{x,\text{PLL}}^{(i)}\right)^2} \tag{43}$$

Substituting $w_{x,\text{PLL}}^{(i)}$ in (24) into (43), (43) can be reformed as

$$\sigma_{x,\text{PLL}} = \sqrt{\frac{1}{\sum_{i=1}^{N_x} \left(\sigma_{x,\text{PLL}}^{(i)}\right)^{-2}}} \tag{44}$$

According to (Julien, 2005; Tran, 2004; Tran & Hegarty, 2002), the theoretical tracking jitter of single-component PLL is

$$\sigma_{x,\text{PLL}}^{(i)} = \frac{\lambda_o^x}{2\pi} \sqrt{\frac{B_n^{\text{PLL}}\left(1 - 0.5B_n^{\text{PLL}}T\right)}{P_x^{(i)}/N_0}\left[1 + \frac{1}{2TP_x^{(i)}/N_0}\right]} \tag{45}$$

Therefore, substituting (45) into (44), theoretical tracking jitter of the PLL is

$$\sigma_{x,\text{PLL}} = \frac{\lambda_o^x}{2\pi} \sqrt{\frac{B_n^{\text{PLL}}\left(1 - 0.5B_n^{\text{PLL}}T\right)}{\sum_{i=1}^{N_x} P_x^{(i)}/N_0}\left[1 + \frac{\sum_{i=1}^{N_x} \frac{P_x^{(i)}/N_0}{2TP_x^{(i)}/N_0+1}}{2T \sum_{i=1}^{N_x} \frac{\left(P_x^{(i)}/N_0\right)^2}{2TP_x^{(i)}/N_0+1}}\right]} \tag{46}$$

Qi *et al. Satellite Navigation* (2024) 5:5

Page 20 of 22

Since the tracking outputs from two PLLs are combined, the theoretical tracking jitter of DMT's carrier tracking according to (26) is

$$\sigma_o = \sqrt{\left(\frac{\lambda_o}{2\lambda_o^l}\right)^2 \sigma_{l,\text{PLL}}^2 + \left(\frac{\lambda_o}{2\lambda_o^u}\right)^2 \sigma_{u,\text{PLL}}^2} \tag{47}$$

Therefore, substituting $\sigma_{l,\text{PLL}}$ and $\sigma_{u,\text{PLL}}$ from (46) into (47), the tracking jitter of carrier tracking loop in (47) can be finally expressed as

where $\bar{x}$ is the complement of $x$, which means that $\bar{x}$ takes the different value with $x$ in the set $\{u, l\}$,

$$\sigma_o = \frac{\lambda_o}{2\pi} \sqrt{\frac{B_n^{\text{PLL}}\left(1 - 0.5 B_n^{\text{PLL}} T\right)}{\sum\limits_{x\in\{u,l\}} \sum\limits_{i=1}^{N_x} \gamma P_x^{(i)}/N_0} \left[1 + \frac{\sum\limits_{x\in\{u,l\}} \alpha_x \left(\left\{\sum\limits_{i=1}^{N_x} \frac{P_x^{(i)}/N_0}{2TP_x^{(i)}/N_0+1}\right\}\left\{\sum\limits_{i=1}^{N_{\bar{x}}} \frac{\left(P_{\bar{x}}^{(i)}/N_0\right)^2}{2TP_{\bar{x}}^{(i)}/N_0+1}\right\}\right)}{2T \prod\limits_{x\in\{u,l\}} \sum\limits_{i=1}^{N_x} \frac{\left(P_x^{(i)}/N_0\right)^2}{2TP_x^{(i)}/N_0+1}}\right]} \tag{48}$$

$$\gamma = \frac{4 \sum\limits_{i=1}^{N_u} P_u^{(i)} \sum\limits_{i=1}^{N_l} P_l^{(i)}}{\left[\sum\limits_{x\in\{l,u\}} \sum\limits_{i=1}^{N_x} P_x^{(i)}\right]^2} \tag{49}$$

and

$$\alpha_x = \frac{\left[\sum\limits_{i=1}^{N_x} P_x^{(i)}\right]^2 + \sum\limits_{i=1}^{N_x} P_x^{(i)} \sum\limits_{i=1}^{N_{\bar{x}}} P_{\bar{x}}^{(i)}}{\left[\sum\limits_{x\in\{l,u\}} \sum\limits_{i=1}^{N_x} P_x^{(i)}\right]^2} \tag{50}$$

**Subcarrier tracking jitter**
According to (37), theoretical tracking jitter of subcarrier tracking in DMT is

$$\sigma_s = \sqrt{\sum_{x\in\{u,l\}} \sum_{i=1}^{N_x} \left(w_{x,\text{SPLL}}^{(i)}\right)^2 \left(\sigma_{x,\text{SPLL}}^{(i)}\right)^2} \tag{51}$$

Substituting $w_{x,\text{SPLL}}^{(i)}$ in (38) to (51), (51) can be simplified as

$$\sigma_s = \sqrt{\frac{1}{\sum\limits_{x\in\{u,l\}} \sum\limits_{i=1}^{N_x} \left(\sigma_{x,\text{SPLL}}^{(i)}\right)^{-2}}} \tag{52}$$

According to (Borio, 2014), tracking jitter of the single-component SPLL is

$$\sigma_{x,\text{SPLL}}^{(i)} = \frac{\lambda_s}{2\pi} \sqrt{\frac{B_n^{\text{SPLL}}\left(1 - 0.5 B_n^{\text{SPLL}} T\right)}{P_x^{(i)}/N_0}\left[1 + \frac{1}{2TP_x^{(i)}/N_0}\right]} \tag{53}$$

Therefore, substituting (53) into (52), DMT's subcarrier tracking jitter can be finally reformed as

$$\sigma_s = \frac{\lambda_s}{2\pi} \sqrt{\frac{B_n^{\text{SPLL}}\left(1 - 0.5 B_n^{\text{SPLL}} T\right)}{\sum\limits_{x\in\{u,l\}} \sum\limits_{i=1}^{N_x} P_x^{(i)}/N_0}\left[1 + \frac{\sum\limits_{x\in\{u,l\}} \sum\limits_{i=1}^{N_x} \frac{P_x^{(i)}/N_0}{2TP_x^{(i)}/N_0+1}}{2T \sum\limits_{x\in\{u,l\}} \sum\limits_{i=1}^{N_x} \frac{\left(P_x^{(i)}/N_0\right)^2}{2TP_x^{(i)}/N_0+1}}\right]} \tag{54}$$

**Code tracking jitter**
According to (32), the theoretical tracking jitter of code tracking in DMT is

$$\sigma_c = \sqrt{\sum_{x\in\{u,l\}} \sum_{i=1}^{N_x} \left(w_{x,\text{DLL}}^{(i)}\right)^2 \left(\sigma_{x,\text{DLL}}^{(i)}\right)^2} \tag{55}$$

Substituting $w_{x,\text{DLL}}^{(i)}$ in (33) to (55), (56) can be reformed as

$$\sigma_c = \sqrt{\frac{1}{\sum\limits_{x\in\{u,l\}} \sum\limits_{i=1}^{N_x} \left(\sigma_{x,\text{DLL}}^{(i)}\right)^{-2}}} \tag{56}$$

According to (Betz & Kolodziejski, 2009a; b), the coherent and non-coherent code tracking jitters of single-component DLL are

$$\sigma_{x,\text{DLL}}^{(i)} = c \sqrt{\frac{B_n^{\text{DLL}}\left(1 - 0.5 B_n^{\text{DLL}} T\right) k_{x,1}^{(i)}}{4\pi^2 k_{x,2}^{(i)} P_x^{(i)}/N_0}} \tag{57}$$

and

Qi *et al. Satellite Navigation*        (2024) 5:5

Page 21 of 22

$$\sigma_{x,\mathrm{DLL}}^{(i)} = c\sqrt{\frac{B_n^{\mathrm{DLL}}\left(1 - 0.5B_n^{\mathrm{DLL}}T\right)k_{x,1}^{(i)}}{4\pi^2 k_{x,2}^{(i)} P_x^{(i)}/N_0}\left[1 + \frac{k_{x,3}^{(i)}}{Tk_{x,4}^{(i)} P_x^{(i)}/N_0}\right]}$$

(58)

respectively, where

$$
\begin{aligned}
k_{x,1}^{(i)} &= \int_{f_o^x - f_r - \beta_r}^{f_o^x - f_r + \beta_r} G_x^{(i)}(f)\sin^2\left(\pi f \mu T_{c,x}^{(i)}\right)\mathrm{d}f \\
k_{x,2}^{(i)} &= \left[\int_{f_o^x - f_r - \beta_r}^{f_o^x - f_r + \beta_r} f G_x^{(i)}(f)\sin\left(\pi f \mu T_{c,x}^{(i)}\right)\mathrm{d}f\right]^2 \\
k_{x,3}^{(i)} &= \int_{f_o^x - f_r - \beta_r}^{f_o^x - f_r + \beta_r} G_x^{(i)}(f)\cos^2\left(\pi f \mu T_{c,x}^{(i)}\right)\mathrm{d}f \\
k_{x,4}^{(i)} &= \left[\int_{f_o^x - f_r - \beta_r}^{f_o^x - f_r + \beta_r} G_x^{(i)}(f)\cos\left(\pi f \mu T_{c,x}^{(i)}\right)\mathrm{d}f\right]^2
\end{aligned}
$$

(59)

and $T_{c,x}^{(i)}$ is a code chip length of $g_x^{(i)}(t)$. Therefore, substituting (57) and (58) into (56), the coherent and non-coherent code tracking jitters of DMT can be finally reformed as

$$\sigma_{c,\mathrm{coh}} = c\sqrt{\frac{B_n^{\mathrm{DLL}}\left(1 - 0.5B_n^{\mathrm{DLL}}T\right)}{4\pi^2 \sum_{x\in\{u,l\}}\sum_{i=1}^{N_x}\frac{k_{x,2}^{(i)}}{k_{x,1}^{(i)}}P_x^{(i)}/N_0}}$$

(60)

and

$$\sigma_{c,\mathrm{noncoh}}$$

$$= c\sqrt{\frac{B_n^{\mathrm{DLL}}\left(1 - 0.5B_n^{\mathrm{DLL}}T\right)}{4\pi^2 \sum_{x\in\{u,l\}}\sum_{i=1}^{N_x}\frac{k_{x,2}^{(i)}}{k_{x,1}^{(i)}}P_x^{(i)}/N_0}\left[1 + \frac{\sum_{x\in\{u,l\}}\sum_{i=1}^{N_x}\frac{k_{x,3}^{(i)}k_{x,2}^{(i)}P_x^{(i)}/N_0}{k_{x,1}^{(i)}\left(Tk_{x,4}^{(i)}P_x^{(i)}/N_0+k_{x,3}^{(i)}\right)}}{T\sum_{x\in\{u,l\}}\sum_{i=1}^{N_x}\frac{k_{x,4}^{(i)}k_{x,2}^{(i)}\left(P_x^{(i)}/N_0\right)^2}{k_{x,1}^{(i)}\left(Tk_{x,4}^{(i)}P_x^{(i)}/N_0+k_{x,3}^{(i)}\right)}}\right]}$$

(61)

respectively.

## Acknowledgements
Not applicable.

## Declarations

## References

Betz, J. W., & Kolodziejski, K. R. (2009). Generalized theory of code tracking with an early-late discrim inator part II: Noncoherent processing and numerical results. *IEEE Transactions on Aerospace and Electronic Systems, 45*(4), 1557–1564. https://doi.org/10.1109/TAES.2009.5310317

Betz, J. W., & Kolodziejski, K. R. (2009). Generalized theory of code tracking with an early-late discrimi nator part I: Lower bound and coherent processing. *IEEE Transactions on Aerospace and Electronic Systems, 45*(4), 1538–1556. https://doi.org/10.1109/TAES.2009.5310316

Borio, D. (2014). Double phase estimator: New unambiguous binary offset carrier tracking algorithm. *IET Radar, Sonar & Navigation, 8*(7), 729–741. https://doi.org/10.1049/iet-rsn.2013.0306

Chen, H., Wang, R., Jia, W., Ren, J., & Yao, M. (2013). An unambiguous tracking method based on pseudo correlation function for AltBOC (15, 10) signal. *Wireless Personal Communications, 69*(4), 1347–1364. https://doi.org/10.1007/s11277-012-0637-z

Dunn, M. J., & Disl, D. (2019). Global Positioning System Directorate Systems Engineering & Integration Interface Specification IS-GPS-200k. Retrieved Mar 4, 2019, from https://www.gps.gov/technical/icwg/meetings/2019/05/Draft-IS-GPS-200K-Mar2019.pdf

Gao, Y., Yao, Z., & Lu, M. (2019). Design and implementation of a real-time software receiver for BDS-3 signals. *Navigation, 66*(1), 83–97. https://doi.org/10.1002/navi.290

Gao, Y., Yao, Z., & Lu, m. (2020a). A coherent processing technique with high precision for BDS B1I and B1C signals. *China satellite navigation conference* (pp. 537–550).

Gao, Y., Yao, Z., & Lu, M. (2020b). Exploring the ultra-high-precision ranging potential of BDS B1 signal. *Proceedings of the 33rd international technical meeting of the satellite division of the institute of navigation (ION GNSS+ 2020)* (pp. 3626–3646).

Gao, Y., Yao, Z., & Lu, M. (2020). High-precision unambiguous tracking technique for BDS B1 wideband composite signal. *NAVIGATION: Journal of the Institute of Navigation, 67*(3), 633–650. https://doi.org/10.1002/navi.377

Hameed, M. S., Woerz, T., Pany, T., Wendel, J., Paonni, M., & Senni, T. (2021). Demonstration of meta signal positioning using LAMBDA ambiguity fixing method within a bit-true simulation. *Proceedings of the 34th international technical meeting of the satellite division of the institute of navigation (ION GNSS+ 2021)* (pp. 2819–2837).

Hein, G. W. (2020). Status, perspectives and trends of satellite navigation. *Satellite Navigation, 1*(1), 1–12. https://doi.org/10.1186/s43020-020-00023-x

Hodgart, M., & Simons, E. (2012). Improvements and additions to the double estimation technique. In *2012 6th ESA workshop on satellite navigation technologies (navitec 2012) & European workshop on GNSS signals and signal processing* (pp. 1–7).

Julien, O. (2005). Carrier-phase tracking of future data/pilot signals. In *Proceedings of the 18th international technical meeting of the satellite division of the institute of navigation (ION GNSS 2005)* (pp. 113– 124).

Lestarquit, L., Artaud, G., & Issler, J.-L. (2008). AltBOC for dummies or everything you always wanted to know about AltBOC. In *Proceedings of the 21st international technical meeting of the satellite division of the institute of navigation (ION GNSS 2008)* (pp. 961–970).

Qi *et al. Satellite Navigation*          *(2024) 5:5*

Page 22 of 22

Linty, N., Bhuiyan, M. Z. H., & Kirkko-Jaakkola, M. (2020). Opportunities and challenges of Galileo E5 wideband real signals processing. In *2020 international conference on localization and gnss (ICL-GNSS)* (pp. 1–6).

Lu, M., Li, W., Yao, Z., & Cui, X. (2019). Overview of BDS III new signals. *Navigation, 66*(1), 19–35. https://doi.org/10.1002/navi.296

Qi, Y., Yao, Z., Gao, Y., & Lu, M. (2022). Robust unambiguous ranging technique for BDS-3 B1 wideband composite signals. *GPS Solutions, 26*(4), 1–15. https://doi.org/10.1007/s10291-022-01296-2

Qi, Y., Yao, Z., & Lu, M. (2023). Carrier Assisted Robust Unambiguous Positioning Technique for Subcarrier Modulated Signals in GNSS. *IEEE Transactions on Vehicular Technology.* https://doi.org/10.1109/TVT.2023.3282291

Rebeyrol, E., Julien, O., Macabiau, C., Ries, L., Delatour, A., & Lestarquit, L. (2007). Galileo civil signal modulations. *GPS Solutions, 11*(3), 159–171. https://doi.org/10.1007/s10291-006-0047-3

Ren, J., Jia, W., Chen, H., & Yao, M. (2012). Unambiguous tracking method for alternative binary offset carrier modulated signals based on dual estimate loop. *IEEE Communications Letters, 16*(11), 1737–1740. https://doi.org/10.1109/LCOMM.2012.092112.121853

Shivaramaiah, N. C., & Dempster, A. G. (2009). A novel extended tracking range DLL for AltBOC signals. In*2009 IEEE 70th vehicular technology conference fall* (pp. 1–5).

Shivaramaiah, N. C., Dempster, A. G., & Rizos, C. (2009). Hybrid tracking loop architectures for the Galileo E5 signal. In *Proceedings of the European navigation conference on global navigation satellite systems ENC GNSS*.

Tawk, Y., Botteron, C., Jovanovic, A., & Farine, P.-A. (2012). Analysis of Galileo E5 and E5ab code tracking. *GPS Solutions, 16*(2), 243–258. https://doi.org/10.1007/s10291-011-0226-8

Tran, M. (2004). Performance evaluations of the new GPS L5 and L2 civil (L2C) signals. *Navigation, 51*(3), 199–212. https://doi.org/10.1002/j.2161-4296.2004.tb00351.x

Tran, M., & Hegarty, C. (2002). Receiver algorithms for the new civil GPS signals. In: *Proceedings of the 2002 national technical meeting of the institute of navigation* (pp. 778–789).

Wang, C., Cui, X., Ma, T., Zhao, S., & Lu, M. (2017). Asymmetric dual-band tracking technique for optimal joint processing of BDS B1I and B1C signals. *Sensors, 17*(10), 2360. https://doi.org/10.3390/s17102360

Wendel, J., Schubert, F., & Hager, S. (2014). A robust technique for unambiguous BOC tracking. *NAVIGATION: Journal of The Institute of Navigation, 61*(3), 179–190. https://doi.org/10.1002/navi.62

Wu, W., Guo, F., & Zheng, J. (2020). Analysis of Galileo signal-in-space range error and positioning perfor mance during 2015–2018. *Satellite Navigation, 1*(1), 1–13. https://doi.org/10.1186/s43020-019-0005-1

Yan, T., Qu, B., Wang, Y., Wang, G., Lei, W., Bian, L., & Meng, Y. (2018). Weighted discriminator function based unambiguous tracking method for dual-frequency constant envelope modulated signals. *Wireless Personal Communications, 103*(3), 1895–1925. https://doi.org/10.1007/s11277-018-5887-y

Yao, Z., Cui, X., Lu, M., & Feng, Z. (2009). Dual update-rate carrier tracking technique for new generation global navigation satellite system signals in dynamic environments. *IET Radar, Sonar & Navigation, 3*(3), 203–213. https://doi.org/10.1049/iet-rsn:20080059x

Yao, Z., Guo, F., Ma, J., & Lu, M. (2017). Orthogonality-based generalized multicarrier constant envelope multiplexing for DSSS signals. *IEEE Transactions on Aerospace and Electronic Systems, 53*(4), 1685–1698. https://doi.org/10.1109/TAES.2017.2671580

Yao, Z., Ma, J., Zhang, J., & Lu, M. (2017). Multicarrier constant envelope composite signal-a solution to the next generation satellite navigation signals. In *Proceedings of the 30th international technical meeting of the satellite division of the institute of navigation (ION GNSS+ 2017)* (pp. 1520–1533).

Yao, Z., Zhang, J., & Lu, M. (2016). ACE-BOC: Dual-frequency constant envelope multiplexing for satellite navigation. *IEEE Transactions on Aerospace and Electronic Systems, 52*(1), 466–485. https://doi.org/10.1109/TAES.2015.140607

Zhou, Y., & Pan, Y. (2014). Unambiguous tracking method for alternative binary offset carrier modulated signals based on pseudo correlation function technique. *IEEE Communications Letters, 19*(3), 371–374. https://doi.org/10.1109/LCOMM.2014.2385076

Zhu, Y., Cui, X., & Lu, M. (2015). Dual binary phase-shift keying tracking method for Galileo E5 AltBOC (15, 10) signal and its thermal noise performance. *IET Radar, Sonar & Navigation, 9*(6), 669–680. https://doi.org/10.1049/iet-rsn.2014.0349

## Publisher's Note